Targeting ARF4-mediated intracellular transport as broad-spectrum antivirals

Cheng-Feng Qin

qincf@bmi.ac.cn

State Key Laboratory of Pathogen and Biosecurity, Beijing Institute of Microbiology and Epidemiology
https://orcid.org/0000-0002-0632-2807

Ming-Yuan Li

Department of Chemical Pathology and Li Ka Shing Institute of Health Sciences, Chinese University of Hong Kong

Kao Deng

State Key Laboratory of Pathogen and Biosecurity, Beijing Institute of Microbiology and Epidemiology

Xiao-He Cheng

State Key Laboratory of Pathogen and Biosecurity, Beijing Institute of Microbiology and Epidemiology

Lewis Yu-Lam Siu

HKU-Pasteur Research Pole, School of Public Health, Li Ka Shing Faculty of Medicine, The University of Hong Kong

Trupti Shivaprasad Naik

HKU-Pasteur Research Pole, School of Public Health, Li Ka Shing Faculty of Medicine, The University of Hong Kong

Viktoriya G Stancheva

Sir William Dunn School of Pathology, University of Oxford,

Peter Cheung

peter.cheung@live.ca https://orcid.org/0000-0001-8474-2906

Zhuo-Ran Gao

Department of Chemical Pathology and Li Ka Shing Institute of Health Sciences, Chinese University of Hong Kong

Qi Wen Teo

University of Illinois at Urbana-Champaign

Sophie Wilhelmina van Leur

Sir William Dunn School of Pathology, University of Oxford https://orcid.org/0000-0002-0411-6102

Ho-Him Wong

HKU-Pasteur Research Pole, School of Public Health, Li Ka Shing Faculty of Medicine, The University of Hong Kong

Yun Lan

Centre for Immunology & Infection, Hong Kong Science and Technology Park https://orcid.org/0000-0002-0302-6893

Na-Na Zhang
Academy of Military Medical Sciences

Yue Zhang
State Key Laboratory of Pathogen and Biosecurity, Beijing Institute of Microbiology and Epidemiology, Academy of Military Medical Sciences

Tian-Shu Cao
State Key Laboratory of Pathogen and Biosecurity, Beijing Institute of Microbiology and Epidemiology, Academy of Military Medical Sciences

Fan Yang
Shenzhen Center for Disease Control and Prevention

Yong-Qiang Deng
Beijing Institute of Microbiology and Epidemiology https://orcid.org/0000-0002-2306-1039

Sumana Sanyal
University of Oxford https://orcid.org/0000-0002-6230-5366

Article

Keywords:

Posted Date: March 11th, 2024

DOI: https://doi.org/10.21203/rs.3.rs-4017169/v1

Additional Declarations: Yes there is potential Competing Interest. C.F.Q. and M.Y.L. have filed a patent related to the finding reported in this paper.

Title page

Targeting ARF4-mediated intracellular transport as broad-spectrum antivirals

Ming-Yuan Li[1,2#], Kao Deng[1#], Xiao-He Cheng[1#], Lewis Yu-Lam Siu[3], Trupti Shivaprasad Naik[3], Viktoriya G Stancheva[4], Peter Pak-Hang Cheung[2], Zhuo-Ran Gao[2], Qi-Wen Teo[3], Sophie van Leur[4], Ho-Him Wong[3], Yun Lan[2,5], Na-Na Zhang[1], Yue Zhang[1], Tian-Shu Cao[1], Fan Yang[6], Yong-Qiang Deng[1], Sumana Sanyal [4*] and Cheng-Feng Qin [1,7*].

Affiliations

1 State Key Laboratory of Pathogen and Biosecurity, Beijing Institute of Microbiology and Epidemiology, Academy of Military Medical Sciences, Beijing 100071, China.

2 Department of Chemical Pathology and Li Ka Shing Institute of Health Sciences, Chinese University of Hong Kong, Hong Kong SAR, China

3 HKU-Pasteur Research Pole, School of Public Health, Li Ka Shing Faculty of Medicine, The University of Hong Kong, Hong Kong SAR, China.

4 Sir William Dunn School of Pathology, University of Oxford, South Parks Road, Oxford OX1 3RE, UK.

5 Centre for Immunology & Infection, Hong Kong Science and Technology Park, Hong Kong SAR, China

6 Institute of Pathogenic Biology, Shenzhen Center for Disease Prevention and Control, Shenzhen, China

7 Research Unit of Discovery and Tracing of Natural Focus Diseases, Chinese Academy of Medical Sciences, Beijing 100071, China

[#]These authors contributed equally to this work and shared the first authorship.

*Corresponding author: Cheng-Feng Qin (qincf@bmi.ac.cn) and Sumana Sanyal (sumana.sanyal@path.ox.ac.uk)

Summary

Host factors that regulate cellular vesicular trafficking also contribute to progeny virions' destination, thus representing as potential antiviral drug targets. Here we demonstrate that genetic deletion of ARF4, a regulator in vesicle transport, repressed multiple pathogenic RNA viral infections including Zika virus (ZIKV), influenza A virus (IAV), SARS-CoV-2 and Vesicular Stomatitis virus (VSV). ARF4 activation was stimulated upon viral infection, and viral production was rescued when reconstituted with the activated ARF4, but not the inactivated mutants. Mechanically, ARF4 deletion obstructed viral normal translocation into Golgi complex, but led to mis-sorting for lysosomal degradation, consequently caused the blockage of final release. More importantly, ARF4 targeting peptides achieved significant therapeutic efficacy against ZIKV and IAV challenge in mice by blocking ARF4 activation. Hence, we clarify the critical role of ARF4 during viral infection, providing a broad-spectrum antiviral target and the basis for further pharmaceutical development.

Introduction

Due to the lack of effective vaccines or antiviral medications, pathogenic RNA viruses like flaviviruses, coronaviruses, and influenza viruses cause epidemics and pandemics [1-5]. RNA viruses have a higher mutation rate than DNA viruses, which causes rapid evolution and drug resistance. Thus, traditional antiviral approaches that target viral proteases/polymerases to inhibit the function of viral proteins encounter difficulties[6,7]. Antiviral medications that target host dependency factors are therefore compelling substitute tactics. Viruses frequently exhibit overlap when it comes to manipulating host cellular functions. Thus, broad-spectrum antiviral potentiality is presented by inhibitors that target important host factors, such as previously published human Dihydroorotate dehydrogenase (DHODH) [8,9]. Since selected host factors usually are indispensable in their own biological processes, a major limitation of this approach is drug safety which make the drug selectivity is difficulty.[10-13]. Therefore, ideal host targets should be sequestered in normal cellular processes or be replaceable with their highly homologous analogues. Lastly, limited knowledge on the mechanisms underlying viral manipulation of host cell biology and biochemical underpinnings of host-pathogens interactions have continued to impede the development of novel antiviral approaches.

The ADP-ribosylation factors (ARFs), which are small GTPases that belong to the Ras superfamily, are known to control intracellular vesicular transport and organelle structure [14]. ARFs are activated upon GTP binding, which enables them to be recruited to intracellular membranes, such as the plasma membrane and other organelles [15]. According to the identity of their amino acid sequences, mammalian ARFs are classified into three classes: Class I ARF proteins (ARF1-3), Class II (ARF4-5), and Class III (ARF6) [14]. Previously, mouse hepatitis coronavirus and the coxsackievirus were evidenced to hijack and manipulate the ARF1 associated signalling pathway [16,17]. With high sequence conserevtion, ARF4 and ARF5 have confounded efforts to define the individual roles of these ARFs. By enlisting coat components and packaging cargo for transport to post-Golgi compartments, they are expected to aid in early Golgi transport [14]. Our previous study has shown that Class II ARFs are involved in secretion of Dengue virus (DENV), a member of flaviviruses [18,19]. However, the exact role of Class II ARFs during RNA viruses infection remains to be investigated.

In this study, we show that ARF4, but not ARF5, was essential for infection and pathogenesis of multiple pathogenic RNA viruses, including ZIKV, IAV, SARS-CoV-2 and VSV. Mechanism studies revealed that the activation of ARF4 guided exact sorting and intracellular transport of progeny virions. Most importantly, ARF4-targeting peptides that were designed to block its activation showed a pan- antiviral effect in both *in vitro* and *in vivo* systems. Thus, the pivotal function of ARF4 exposes a critical vulnerability in the infection of RNA viruses which provides the foundation for broad-spectrum antivirals against human diseases.

Results

ARF4, not ARF5, is vital for *in vitro* and *in vivo* ZIKV infection

To clarify the role of class II ADP-ribosylation factors (ARF4 and ARF5) in the infection of ZIKV, we generated CRISPR-Cas9 mediated knock-out of ARF4 and ARF5 in Vero cells respectively (**Fig. 1a**), and then challenged with ZIKV. ARF4, but not ARF5 deletion was found to protect cells from ZIKV induced cytopathic effect (CPE), implying a vital role of ARF4 in ZIKV infection (**Fig. 1b**). Production of ZIKV progeny virions was dramatically reduced (~2-4 logs) in ARF4 knock-out ($ARF4^{-/-}$), but not ARF5 knock-out ($ARF5^{-/-}$) cells compared to wild type (WT) cells (**Fig. 1c**). In addition, ZIKV secretion was stalled in $ARF4^{-/-}$ cells, emphasising the critical role of ARF4 in the ZIKV infectious life cycle (**Fig. 1c**).

To further investigate the importance of ARF4 *in vivo*, we utilized Cre-loxP system to generate tissue specific knock-out ARF4-flox/cre-Prok2 (fl+Prok2) mice. Transcription of ARF4, but not ARF5 was largely reduced in the two main ZIKV-targeting tissues-brain and testis (**Fig. 1d and Extended Data Fig.1**). Mice were pre-treated with an anti-mouse IFNAR1 antibody a day before ZIKV challenge, which suppressed type I IFN responses, facilitating successful ZIKV infection and associated pathogenesis **(Fig. 1e)** [20]. Therefore, this ZIKV infection mouse model was used for subsequent animal infection experiments. Compared to ARF4-flox (fl) control mice, ZIKV induced viremia measured in serum samples at 2, 4, and 6 days p.i. was significantly restrained in fl+Prok2 mice **(Fig. 1f).** As expected, viral load in brain and testis of fl+Prok2 mice were measured to be substantially reduced, particularly at day 6 post infection (**Fig. 1g,h**). Importantly, inflammatory cell infiltration in brain, typically associated with ZIKV induced

pathogenesis, was absent in fl+Prok2 mice (**Fig. 1i left panel**). Moreover, necrotic seminiferous tubules, another ZIKV induced pathological abnormality, were observed in testis of ZIKV infected control mice, but not in fl+Prok2 mice (**Fig. 1i right panel**). Collectively, these data demonstrate that ARF4 is a vital host factor that facilitate its infection *in vitro* and *in vivo*.

ZIKV activates ARF4 to facilitate replication

Subsequent investigations were aimed at determining the underpinnings of ARF4 function in ZIKV infection. ARF4 is known to switch between its active GTP-bound form and inactive GDP-bound form. To ascertain the status of ARF4 during ZIKV infection, activated ARF4 were pulled down and measured by using GST fused GGA3 VHS-GAT **(Fig. 2a)** [15]. Results showed that ZIKV infection led to significant increase in activated ARF4 compared with the mock group**(Fig. 2b,c)**. To test whether ZIKV infection relies on the activation of ARF4, we reconstituted and stably expressed wide type ARF4, as well as two mutants-T31N and Q71I into the ARF4$^{-/-}$ cells which maintained ARF4 in inactivated and activated states respectively **(Fig. 2d)** [15]. All reconstituted ARF4 WT and mutants were expressed to similar levels in ARF4$^{-/-}$ cells (**Fig. 2e**). ZIKV infection was performed in these genetically modified cells together with their parental ARF4$^{-/-}$ and Vero cells as a negative and positive controls respectively. Plaque assay results showed that, compared to the viral titer measured in WT and ARF4$^{-/-}$ samples, production of progeny virus was efficiently rescued in ARF4 WT and Q71I expressing cells, but not in T31N expressing cells (**Fig. 2f**), indicating that ZIKV infection relies on the activation of ARF4. To confirm it, ARF4 WT and T31N were stably overexpressed in Vero cells and then challenged by ZIKV (**Fig. 2g,h**). Vero ARF4-Q71I expressing cells were failed to be conducted which overexpressed activated ARF4 would be toxic to cells. As expected, the number of produced progeny virions was slightly escalated in ARF4 WT overexpressing cells, in contrary, significantly restrained in T31N overexpressing cells (**Fig. 2i**). Our data therefore demonstrates that ZIKV infection leads to the activation of endogenous ARF4, which in turn, facilitates its subsequent life cycle.

ARF4 alone harmonizes intracellular transport and secretion of progeny virions.

Our previous studies clued that combination of ARF4 and ARF5 might affecte the secretion of another member of flavivirus-DENV [19]. Therefore, we tested whether ARF4 alone

would regulate the egress of ZIKV. We stably expressed ZIKV structural proteins-prM and E and isolated single clones in Vero WT and ARF4$^{-/-}$ cells respectively (**Fig. 3a**). Stably expressed ZIKV prM and E have been confirmed to form non-infectious recombinant subviral particles (RSPs) which traffic along the same compartments as infectious ZIKV [18,21]. Although similar levels of ZIKV E proteins were expressed in both WT and ARF4$^{-/-}$ cell lysate (CL), E protein was rarely detected in supernatants (SN) collected from ARF4$^{-/-}$ cells (**Fig. 3b**). RSP secretion were calculated as the percentage of secreted E in SN to total E proteins (CL+SN) indicating that release of ZIKV RSPs was almost completely blocked in the absence of ARF4 (**Fig. 3c**).

To further investigate whether ARF4 deletion interfered with viral assembly in ER membrane, we employed transmission electron microscopy (TEM) to visualize newly formed progeny virions. Compared to wild-type cells, ARF4-deficiency did not change the viral assembly. Viral particles measuring approximately 50nm electron-dense dots were observed either in the ER lumen, or packaged into a vesicle generated by ER invaginations (**Fig. 3d and Extended Data Fig.2**). we performed freeze-and-thaw (F&T) assay in the RSP-producing cells to quantify the abundance of RSP formation[22]. Soluble and membrane fractions containing assembled virions and free viral structural proteins were separated using specific markers (**Fig. 3e**). The percentage of E in cytosol fraction to the total amount (cytosol + membrane) was used as an index of virion formation. Our data revealed that 64.2% of E protein was detected in assembled virions in ARF4-deficient cells, more than double that of wild-type cells (**Fig. 3f**). These data indicate that ARF4 does not participate in viral assembly but in subsequent intracellular transport, arresting newly formed viral particles in the deficient cell.

Considering the rate-limiting step in intracellular transport of progeny ZIKV is ER-to Golgi transport and trafficking across Golgi complex, we co-stained the viral E protein together with either trans-Golgi network marker-TGN46 or cis-Golgi marker-GM130 in ZIKV infected and RSP-producing cells respectively. E-stained condensed structures were observed, partially co-localizing with TGN46 or GM130 -stained Golgi complex, indicating arrival of newly assembled viral particles into the Golgi complex (**Fig. 3g, i upper panel**). In contrast, the E-stained membranes were fragmented and rarely localized to the Golgi in the ARF4$^{-/-}$ cells (**Fig. 3g, i lower panel**). Further image analysis demonstrated that the percentage of E protein co-localized with Golgi apparatus was more than 50% reduced in ARF4$^{-/-}$ cells compared to WT cells (**Fig3h, k**). Collectively, these data indicates that ARF4 harmonizes sorting newly formed

viral particles into the "correct" intracellular trafficking routes to achieve a successful viral maturation and egress.

ARF4 deficiency leads to mis-sorting of progeny virions.

Interestingly, our TME observations revealed that in ZIKV infected Vero cells, virion embedded vesicles accumulated as a clusters (pointed by blue star) either into early endosome (EE) like vesicles (**Fig. 4a and Extended Data Fig.3 upper panel**) or were being released from the cell surface (**Fig. 4b and Extended Data Fig.4 upper panel**). However, in ARF4$^{-/-}$ cells, similar clusters and free virions (pointed by red arrow) were more frequently in late endosome/multivesicular bodies (MVBs) like vesicles surrounded by lysosomes, an indicative of degradation. (**Fig. 4a and Extended Data Fig.3 lower panel**). Although similar membrane protrusions were observed in either ZIKV infected ARF4$^{-/-}$ or uninfected WT/ARF4$^{-/-}$ cells, the latter were devoid of any virions (**Figure 4b and Extended Data Fig.4**). Moreover, transcriptome analysis by performing RNA-Seq using ZIKV infected WT or ARF4$^{-/-}$ cells also indicated that genes relative to lysosomal degradation were enriched by GO analysis (**Fig. 4c**) and up-regulated in ARF4 $^{-/-}$ cells (**Extended Data Fig.5**). Therefore, we speculated that ARF4-deficiency results in mis-sorting of virions into late endosomes/MVBs, for subsequent degradation in the lysosomes. To test this hypothesis, lysosomal degradation was inhibited in ARF4$^{-/-}$ cells by using lysosome inhibitor-chloroquine. Results showed that, comparing to ZIKV infected WT cells, viral egress was recovered in ARF4$^{-/-}$ cells upon chloroquine treatment to block lysosomal degradation but not with MG132 to block proteasome degradation (**Fig. 4d**). In addition, upon ZIKV infection, a higher expression of EEA1, as early endosome marker was specifically detected in WT cells, whereas an increased expression of LAMP2, as late endosome marker was detected in ARF4$^{-/-}$ cells (**Fig. 4e**). Then, we performed immunofluorescence imaging by co-staining viral E protein with EEA1 or LAMP2. Distribution of endogenous EEA1 was dispersed into smaller puncta throughout the cytoplasm in ZIKV infected WT cells, but not in ARF4$^{-/-}$ cells or mock infected cells where EEA1 was accumulated as cytosolic foci at perinuclear regions (**Fig. 4f**). In contrast, distribution of lysosomes as detected by LAMP2 was expanded throughout the cytoplasm in ZIKV infected ARF4-deficient, but not in WT cells (**Fig. 4h**). Moreover, image analysis indicated that more ZIKV E protein was co-stained with EEA1 in WT cells, whereas with LAMP-2 in ARF4$^{-/-}$ cells (**Fig. 4g,i**). These results

demonstrated that ARF4-deficiency resulted in aberrant intracellular sorting and transport of virions, consequently triggering their lysosomal degradation instead of being released.

ARF4 is vital for multiple pathogenic RNA viruses.

To test whether ARF4 was also required by other pathogenic RNA viruses, we tested a range of pathogens. Our data showed that secretion of chosen RNA viruses, including IAV, SARS-CoV-2 and VSV, was substantially reduced in ARF4-deficient cells (**Fig. 5a**). To further investigate the importance of ARF4 in other RNA virus infections in vivo, we established heterozygous ARF4 knock-out ($ARF4^{-/+}$) mice, with > 60% reduction of ARF4 mRNA in the lung and trachea, for IAV challenge (**Fig. 5b**). As shown in **Fig. 5c**, a lethal dose of IAV was intranasally administrated into $ARF4^{-/+}$ and its control wide-type (WT) mice. Although body weight loss were observed in both WT and $ARF4^{-/+}$ mice post IAV infection, $ARF4^{-/+}$ mice (6/8) started to regain weight at 9 days p.i. and recovered at 14 days p.i. in comparison to control WT mice (2/8) (**Extended Data Fig.6**). Survival analysis revealed that ARF4 reduction resulted in significant increase from 25% in control to 75% in $ARF4^{-/+}$ mice (**Fig. 5d**). Moreover, viral loads measured in tracheal and lung showed nearly 90% and 70% reduction in $ARF4^{-/+}$ mice (**Fig. 5e,f**). Besides, ARF4 depletion also eliminated the typical IAV induced histopathological changes, such as thickness of alveolar septum and fluid exudation in alveolar cavities, accompanied by inflammatory cell infiltration[23,24] (**Fig. 5g,h**). Collectively, our investigation confirmed that ARF4 plays a vital role in multiple RNA viruses infection and pathogenesis.

ARF4 is a broad spectrum antiviral target

Since data from our above studies indicated ARF4 as a potential antiviral target against pathogenic RNA viruses, we designed peptides targeting human ARF4 to test their effect in viral infection. Previous studies have indicated that the C-terminal motif, VXPX-COOH, of rhodopsin regulates its intracellular trafficking by binding to and activating endogenous ARF4[25], therefore five peptides, named **ARF4 T**argeting **P**eptide 1-5 (ARF4TP 1-5) basing on the VXPX sequence, were designed and synthesized as detailed in **Fig. 6a**. Their 50% cytotoxicity concentration (CC_{50}) and the half maximal inhibitory concentration (IC_{50}) of ZIKV production were measured by MTT and RT-qPCR respectively. ARF4TP-4 was selected with the most effective inhibition of ZIKV production (IC_{50} of 3.25 μM), while displaying low cytotoxicity

(CC_{50} of 196.2 μM) (**Fig. 6a**). VHS-GAT fused GST-pull down results showed that ARF4 activation was not stimulated by ZIKV infection when treated with ARF4TP-4 (**Fig. 6b-d**), verifying our hypothesis that ARF4TP-4 inhibits ZIKV infection by blocking ARF4 activation**.**

A published study demonstrated that interaction of GBF1 is indispensable for ARF4 activation to form GBF1-ARF4 complex [25]. We, therefore, established the models of ARF4 in complex with GBF1 and ARF4TP-4 by utilizing molecular docking. As indicated in **Extended Data Fig.7a**, the ARFTP-4 could bind to the groove composed by ARF4 (WT and Q71I) and GBF1 with docking energy of -7.77 kcal/mol of ARF4 WT-GBF1-ARF4TP-4 and -6.94 kcal/mol of ARF4 Q71I-GBF1-ARF4TP-4. However, the inactivated ARF4-T31N mutant is unable to form dimer with GBF1, thus fail to bind to ARFTP-4. Since ARF4TP-4 binds the activated ARF4-Q71I mutant, we tested its effect on ZIKV production when ARF4 had been stimulated. Results showed that ZIKV secretion was not sensitive to ARF4TP-4 treatment in ARF4-Q71I expressing cells, analogous to the response in ARF4-deleted cells (**Extended Data Fig.7b**). On the other hand, ARF4TP-4 dependent inhibition was rescued when wild type ARF4 was reconstituted into $ARF4^{-/-}$ cells (**Extended Data Fig.7b**).

As expected, ARF4TP-4 functioned in viral secretion. Comparing to the none-treated cells, 5μM ARF4TP-4 was sufficient to cause 75% reduction of RSPs production and almost fully blocked when concentration was up to 20μM **(Fig. 6e-f)**. To verify the antiviral effect of ARF4TP-4 in other RNA pathogenic viruses, we measure the IAV titration in the presence of ARF4TP-4. We performed an order-of-addition experiment either with full time (FT) treatment which was pre-treated 4hrs before infection and maintained in the whole infection or with post infection (PI) treatment which was only added at 4hrs post infection **(Fig. 6g)**. Results showed that ARF4TP-4 was efficiently suppressed IAV infection with dose-dependent **(Fig. 6h).** Moreover, ARF4TP-4 also functions in post entry steps of the IAV infectious life cycle **(Fig. 6h)**. Collectively, our data confirm that competitive binding of ARF4TP-4 to endogenous ARF4 interferes with ARF4 activation, subsequently blocking viral production.

ARF4TP-4 treatment is safe and confers protection against ZIKV and IAV challenge in mice

Lastly, to evaluate the *in vivo* efficacy of ARF4TP-4, we first assessed the safety of ARF4TP-4 in mice. ARF4TP-4 was administered daily via intraperitoneal (IP) injection thrice, with an increasing dose from 10 to 160 mg kg^{-1} of body weight (**Extended Data Fig.8a**). In comparison

to the PBS vehicle group, administration of ARF4TP-4 did not affect body weight nor induce any abnormal behaviour (**Extended Data Fig. 8b**). Furthermore, the levels of alanine aminotransferase (ALT) (**Extended Data Fig. 8c**) and creatinine in sera (**Extended Data Fig. 8d**), which serve as indices of hepatic and renal function respectively, displayed no significantly changes upon ARF4TP-4 administration. Neither did Haematoxylin-and-eosin (HE) staining of sections of brain, heart, liver, spleen, lung, kidney and testis display any pathological abnormality regardless of PBS or ARFTP-4 treatments at varying doses (**Extended Data Fig. 8e**). ARF4TP-4 was therefore deemed safe for mice, even at the highest dosage of 160mg kg^{-1} of body weight.

Then, to evaluate ARF4TP-4 as a potential antiviral agent, C57BL/6 mice were i.p. administrated thrice daily with ARF4TP-4 ZIKV challenge was conducted a day after the third ARF4TP-4 (**Fig. 6i**). ZIKV induced viremia was significantly eliminated in ARF4TP-4 pre-treated group in compared to the vehicle group (**Fig. 6j**). Crucially, ZIKV infection was efficiently inhibited in the testis of ARF4TP-4 pre-treated mice, where the viral load was reduced by 65.52 % at day 2 p.i. and almost 90% at day 6 p.i. (**Fig. 6k**). Simultaneously, pathologies such as necrosis, haemorrhage and exudate deposits in the lumen of seminiferous tubules, were abolished in the ARF4TP-4 treated group (**Extended Data Fig. 9**).

Lastly, we further evaluated the efficacy of ARF4TP-4 against IAV challenge. C57BL/6 mice were pre-treated with ARF4TP-4 or PBS once before IAV challenge, followed by three subsequent administrations post IAV intranasal inoculation(**Fig. 6l**). Body weight monitoring suggested that ARF4TP-4 could efficiently protect mice from IAV infection, with 4 of 8 mice from the 80mg kg^{-1} treatment group displaying complete protection without significant weight loss post IAV infection (**Extended Data Fig. 10**). The survival rates increased from 25% in the control group to 44.4% in 20mg kg^{-1} treated group, and remarkably up to 75% in 80mg kg^{-1} treated group (**Fig. 6m**). Moreover, ARF4TP-4 treatment efficiently blocked IAV infection in the trachea and lung.(**Fig. 6n-o**). In particular, viral load in the trachea and lung was undetectable in some of the IAV infected mice (3/6) from the 80mg kg^{-1} treatment group, aligning with body weight observation. Similar to the observation in $ARF4^{-/+}$ mice, ARF4TP-4 administration efficiently protected mice from histopathological changes (**Fig. 6p-q**). Altogether, ARF4TP-4 showed a potential broad anti-viral capability warranting further optimization.

Discussion

By utilizing ARF4-deficient cells and edited mice, we provide solid evidence revealing an essential role for the host factor-ARF4 in infection and pathogenesis of multiple RNA viruses, causing seasonal epidemics or worse global pandemics. We characterised ARF4 to show it functions in intracellular vesicle transport, playing an indispensable role in determining the progeny virions destination. Furthermore, ARF4 activation was confirmed to be essential for a successful viral infection. Therefore, ARF4 targeting peptides which efficiently blocked ARF4 activation suppressed viral infection both *in vitro* and *in vivo*, with prevention of histopathological changes in viral targeting tissues.

Vesicle transport between different intracellular organelles is the predominant way for exchange of proteins and lipids in cells, as well as, function in several fundamental biological processes, like secretion and modification along secretory pathway.[26,27]. Vesicular trafficking certainly plays an indispensable role in viral infectious life cycle especially for the final egress stage [28-30]. Here, the host factor-ARF4 was firstly evidenced to be hijacked alone by multiple pathogenic RNA viruses to achieve a successful infection. Our studies confirm that ARF4 deletion or dysfunction by targeting peptides efficiently restrict the proliferation of highly pathogenic viruses, including ZIKV, IAV and newly emerged SARS-CoV-2. ARF4TP-4 also display therapeutic effects in all tested infected mice model. Therefore, This ARF4-dependent characterization reveals a novel viral vulnerability which makes ARF4 as an attractive pan antiviral drug target.

Limited knowledge of intracellular vesicle transport and the mechanisms manipulated by viruses greatly impedes the development of antiviral therapies. Our results firstly demonstrated that virus infection stimulates the ARF4 activation enabling appropriate sorting of progeny virions and regulating their intracellular vesicle transport for egress. According to this discovery, further investigation using a targeting peptide to block ARF4 activation successfully suppress viral infection, as well as relieve viral induced pathogenic changes and reduce lethal death. Thus, therapeutic treatment aiming to the regulation of ARF4 activation is a promising antiviral approach.

Considering to the biological functions of host factors in their own cellular processes, potential toxicity is a main weakness in this approach.[11,31-33]. Published reports show ARF4 prefers to accompany with other ARFs, like ARF1 or ARF5 when functions in intracellular vesicle transport among Golgi complex or along the early secretory pathway[34-36]. This hint that ARF4 alone might not a irreplicable factor to host. Thus, highly evolved, host adapted viruses hijack ARF4 to perform moonlighting functions in the viral lifecycle, while coordinating with their normal role in host biology. Our experimental data convinces this hypothesis which neither ARF4 deletion nor dysfunction caused toxicity in virus susceptible cells and gene-editing mice. ARF4 targeting peptides also have been confirmed to induce extremely low cytotoxicity and was safe used in mice. Altogether, ARF4 inhibitors have promising therapeutic potential as safe and broad-spectrum antiviral drugs, hence deserve a further exploration and turn into translational research.

At last, recent research have uncovered several unconventional vesicle dependent secretion pathways that are utilized by intracellular pathogens to escape circulating antibody and facilitate their dissemination. For instance, flaviviruses, like Dengue and ZIKV[21], as well as enteroviruses[37-39], such as polio, coxsackievirus B and enterovirus 71 were reported to egress via secretory autophagosomes which virion encapsulated autophagosomes are fused with cell membrane instead of lysosome. In contrary, β-Coronaviruses including SARS-CoV2 can exploit lysosomes to initial lysosomal trafficking for egress[40,41]. Our data shown that in ARF4-deleting cells, ZIKV progeny virions were sorted into late-endosome/MVBs surrounding by lysosome which initial the lysosomal degradation. However, ARF4 absence dose not completely arrest the viral egress, thus some unknown bypass, to a large extent, the lysosome involved vesicle trafficking would be hijacked.

Collectively, identification of host ARF4 has revealed a vulnerability in infection by multiple pathogenic RNA viruses, providing a potential broad-spectrum antiviral targeting warranting further investigation to illustrate mechanisms for viral subversion.

Methods

Cells

Knockout ARF4 and ARF5 cells were generated using sgRNA sequences (ARF4: 5'-TCCCTCTTCTCCCGACTATT-3' and 5'- TATCCCTTACCTGGGTATTC-3' ; ARF5: 5'-GAAGATCCGCGAAAAGAGCG-3' and 5'- TGGACAGTAATGACCGGGAG-3') which cloned into the CRISPR/Ca9 vector pX459. Established clone was transfected into Vero cells and puromycin selection was performed after 48hrs transfection at a concentration of 10-12-10μg/ml for 3 days. Single clones were picked by limiting dilution and confirmed by Western blotting using their specific antibodies . The stable cell lines expressing either prME-ZIKV or wild type ARF4 and its mutants were established using the retroviral vector pCHMES-IRES-Hygromycin, selected following a 2 week period in the presence of 500 μg/ml hygromycin and maintained thereafter the same medium. Single clones were picked by limiting dilution and confirmed by Western blotting using their specific antibodies . Above cells were maintained in DMEM supplemented with 10-15% fetal bovine serum (FBS) and 1% penicillin/streptomycin at 37°C, with 5% CO2. Aedes albopictus clone C6/36 was maintained in RPMI 1640 plus 15% FBS.

Viruses

ZIKA virus (NC-14-5132 and GZ01) were propagated in the C6/36 cells and titrated using plaque assay in Vero cells. Influenza A virus (A/WSN/33 H1N1) were grown and titrated using plaque assay in BHK21 cells. Vesicular Stomatitis recombinant Virus and SARS-CoV-2 strains /human/CHN/Beijing_IME-BJ05/2020 (IME-BJ05, accession no. GWHACAX01000000) was propagated and titration using plaque assay in Vero cells.

Mouse studies

All animal experimental procedures were carried out according to ethical guidelines and approval by Institutional Laboratory Animal Care and Use Committee at Beijing Institute of Microbiology and Epidemiology (IACUC-DWZX-2021-034 and IACUC-IME-2022-051). Gene-editing of mice were generated and bred by GemPharmatech Co. LTd. For ARF4 heterozygous knout out mice was also generated via CRISPR-Cas9 system. The brief process is as follows: sgRNA was transcribed in vitro.Cas9 and sgRNA were microinjected into the fertilized eggs of C57BL/6JGpt mice. Fertilized eggs were transplanted to obtain positive F0 mice which were confirmed by PCR and sequencing. A stable F1 generation mouse model was obtained by mating positive F0 generation mice with C57BL/6JGpt mice. For tissue specific knock-out mice: ARF4-flox/cre-Prok2 were established by utilizing Cre-LoxP system to generate ARF4-flox and

Cre-ProK2 C57BL/6JGpt mice via CRISPR-Cas9 system respectively, then the flox mice will be knock out after mating with mice expressing Cre recombinase, resulting in the loss of function of the target gene in specific tissues and cell types. For ARF4TP-4 efficiency assay, The specific pathogen-free wide-type C57BL/6JGpt mice were purchased at Beijing Vitalriver Laboratory Animal Technology Co. Ltd. In ZIKV challenge assay, either wild-type or gene-editing mice (4-6 weeks old) were i.p. administered with an anti-mouse IFNAR1 antibody (2mg/mice) a day before ZIKV challenge to suppress type I IFN responses. Then, $5*10^5$ PFU of ZIKV (GZ01) was infected i.p. To measure viral load, retro-orbitally bled and two main ZIKV targeting tissue-brain and testis were randomly collected from infected mice at indicated day post infection. 6 days post infected brain and testis were randomly collected to be fixed in 4% PFA for further HE staining. In IAV challenge assay, either wild-type or gene-editing mice (8-9 weeks old) were intranasally administrated with $1.5*10^4$ PFU. of IAV (A/WSN/33 H1N1). Body weight changes and mortality were monitored for 14 days. Lung and tracheal from 3 and 6 days p.i. were collected to check viral load. 6 days post infected lung were randomly collected to be fixed in 4% PFA, then sectioned and stained with hematoxylin and eosin (H&E).

Plaque assays to measure virus infection

Serial dilutions of SN from infected cells were added to BHK-21/Vero cell monolayer and adsorbed for 60 min at 37 C. Cells were washed and plaque media was overlaid on the cells and placed at 37 °C. After 3-6 days of incubations, the cell monolayers were stained with crystal violet and plaques were counted.

Reverse transcription-quantitative PCR to measure viral RNA copies

Viral RNA was automatically extracted from viral infected mice sera or targeting tissue by GeneRotex 48 nucleic acid extractor (Tianlong) using viral DNA/RNA extraction kit. Then viral RNA copy numbers were amplified using the One Step PrimeScript RT-PCR kit (TaKaRa RR096a/RR064a). Primers in this study were designed using the Oligo software. ZIKV RNA copies were determined using a specific primer set (ZIKV-ASF: 5'-GGTCAGCGTCCTCTCTAATAAACG-3'; ZIKV-ASR: 5'-GCACCCTAGTGTCCACTTTTTCC-3'). IAV RNA copies were determined using a specific probe (5'-FAM TGCAGTCCTCGCTCACTGGGCACG-MGB-3') and primer set (QFluA-F: 5'-GACCRATCCTGTCACCTCTGAC-3'; QFluA-R: GGGCATTYTGGACAAAKCGTCTACG-3'). Following the manufacturer's protocol, 18 μl reaction

mixtures of the One Step PrimeScript RT-PCR kit with 2 μl of RNA template were used to perform RT-qPCR assays using the LightCycler 480 real-time PCR system (Roche).

RSPs quantification

To identify RSPs secretion efficiency, RSPs producing cells were firstly replaced with FBS free culture medium for overnight starvation, subsequently, changed into OptiMEM without FBS or plus 2.5% FBS to initial RSPs production. After 1 or 2 days recovery of RSPs production, culture medium was collected and spin down at max speed, 2 min at 4 °C . Transparent culture medium was transferred into new tubes as supernatant (SN). Removing leftover culture medium, then washing with cold PBS 1-2 times. Cells were then lysed in cell lysis buffer and cell lysate (CL) was collected after centrifugation at max speed, 15min at 4 °C. Collected SN and CL were added with 30ul 4× NuPAGE LDS sample buffer and subjected to western blotting assay using the specific antibody against ZIKV E proteins. The mean luminescence and area of E protein signals detected in SN and CL were measured by densitometry using ImageJ software.

GST-VHS-GAT pull down assay

The activity of ARF4 was detected by GST-VHS-GAT pull down assay following the published protocol[15]. GST fused VHS-GAT was bacterially expressed and purchased from Sino Biological Inc. Pull down assay were performed by using Pierec™ GST protein interaction pull-down kit (Thermo Scientific). In brief, ZIKV or mock infected Vero cells with or without ARF4TP-4 treatment were lysed using pull-down lysis buffer provided by kit and measured by BCA protein assay kit (Thermo Scientific). 150μg GST-VHS-GAT was firstly incubated with 250μg cell lysate overnight at 4°C, and then added to equilibrate Glutathione Agarose column for additional overnight incubation at 4°C. Arfter washing 1-2 times with 1ml washing solution, agarose slurry was resuspended by 85μl of 2× NuPAGE LDS sample buffe (Thermo Scientific) plus 10μl of 10*reducing buffer (Thermo Scientific) and 5μl 25*proteinase inhibitor. The bound proteins were then eluted and analyzed by Western blotting with anti-ARF4 antibody.

Transmission electron microscopy

Wild-type and ARF4$^{-/-}$ cells were infected with Zika (MOI 10, 24 h), fixed in 2.5% glutaraldehyde, washed three times in PBS and serially dehydrated. The cells were postfixed in 1% osmium tetroxide and embedded in Araldite resin (Polysciences). Blocks were sectioned with a

diamond knife on an ultramicrotome (Leica microsystems) and examined with a transmission electron microscope (CM100, Philips).

Freeze-and-thaw assay

Sub-confluent wide-type or ARF4 knock-out Vero cells stably expressed ZIKV prME were firstly detached in PBS plus 5mM EDTA at 37°C for 5min, then washed with cold PBS of 5mM EDTA for three time. Cells finally were re-suspended in a buffer containing 10% w/v sucrose, 20mM Tris HCl, 150mM NaCl plus protease inhibitors cocktail (Roche), and then subjected to eight cycles of freeze (dry ice) and thaw (37°C water both), 1min each step. Nuclei and cellular debris were removed by a short (5s) spin down at 14,000 RPM, 4°C. Supernatants were collected and centrifugated at 14,000 RPM, 4°C to pellet the membrane fraction which was then re-suspended in cold PBS. The final supernatant ,as cytosol fraction, containing newly formed RSPs, together with re-suspended membrane fraction, containing sole unpacked ZIKV E proteins, were analyzed with western blotting assay using the specific antibody against ZIKV E proteins.

Fluorescence microscopy

For fluorescence microscopy, cells grown on coverslips were fixed in 4% paraformaldehyde for 15 min, permeabilised with 0.1% TX-100 in PBS for 5 min and blocked with 5% goat serum 0.1% TX-100 in PBS for 30 min. Cells were incubated with primary antibodies for 2 h at room temperature, and then probed with appropriate secondary antibodies. Nuclei were stained with DAPI and mounted on glass slides for image acquisition using LSM 700/780 confocal microscope. To determine ZIKV progeny virion or RSP localization in the Golgi apparatus, weighted co-localization coefficients of E with Golgi markers were computed using the ZEN2011 co-localization coefficient software (Carl Zeiss). The sums of intensities of pixels corresponding to anti-E (So) and to co-staining with anti-E and either cis-Golgi or TGN marker (Sc) were computed and then weighted co-localization coefficients, which are equal to the ratio of Sc to So, were used to present the percentage of virions/RSP translocated to either cis-Golgi or TGN.

RNA-sequencing and analysis

For RNA-sequencing assay, total RNAs were extracted from ZIKV or mock infected wild-type and ARF4-/- cells using TRIzol following manufacturer's protocols. RNA concentration and

quality were assessed firstly before RNA-seq. The RNA library construction and high-throughput sequencing were performed by Beijing Annoroad Gene Technology Company. Briefly, multiplexed libraries were sequenced for 150 bp at both ends using an Illumina HiSeq6000 platform. Clean reads were aligned to the green monkey genome (Chlorocebus_sabeus 1.1) using Hisat2 (v2.1.0). The number of reads mapped to each gene in each sample was counted by HTSeq (v0.6.0) and FPKM (Fragments per Kilobase Million) was then calculated to estimate the expression level of genes in each sample. Genes with Padj < 0.05 and |Log2FC| ≥ 1 were identified as DEGs. DEGs were filtered by DESeq2 (v1.40.2) package in R (v4.3.1). GSEA(Gene Set Enrichment Analysis) of all genes and bubble chart were constructed using clusterProfiler (v4.8.3) package in R. Heatmaps of gene expression levels were constructed using pheatmap (v1.0.12) package in R.

Cell cytotoxicity and antiviral inhibition of ARF4 targeting peptides (ARF4TPs)

ARF4TPs were synthesized by Nanjing TGpeptide Biotechnology Co. Ltd and dissolved in PBS to make a 10mM stock. The CellTiter-Glo® Cell Viability Assay (Promega) was employed to evaluate the cytotoxicity according to the manufacturer's protocols. In briefly, Vero cells were treated with different doses of either ARF4TPs or PBS in quadruplicate. Luminescence was recorded after 3 days of incubation at 37 °C, and the 50% cytotoxic concentration (CC50) was calculated using a sigmoidal nonlinear regression function to fit the dose-response curve using GraphPad Prism 7.0 software. To detect antiviral inhibition, a serial diluted ARFTPs were added into overnight attached Vero cells. ZIKV infection was performed at a MOI of 0.1 after 4hrs ARF4TPs treatment and incubated 1hr at 37 °C. After incubation, infected cells were washed three time with PBS, then replenished with fresh culture medium plus indicated diluted ARF4TPs. Viral genomic RNA copy No. from 1 day p.i. supernatant were quantified by RT-qPCR with ZIKV specific primers and 50% inhibition concentration (IC50) was calculated using GraphPad Prism 7.0 software.

ARF4TP4 treatment assay in vivo

For ARFTP-4 treatment in ZIKV infected mice, 3-4 weeks C57BL/6 mice were assigned randomly to two groups and were injected by i.p. route with PBS, or 20mg kg^{-1} ARF4TP-4 daily for three consecutive days. ZIKV challenge were performed a day after first dose ARF4TP-4 injection. As an index of viremia, ZIKV genomic RNA in ZIKV infected mice sera were detected

by RT-qPCR at 2, 4 and 6 days p.i.. Mice were sacrificed at indicated days p.i. for tissue collection for further detection. For ARF4TP-4 treatment in IAV infection in vivo, 8-9 weeks C57BL/6 mice were assigned randomly to three groups and were injected by i.p. route with PBS, 20mg kg^{-1} or 80mg kg^{-1} ARF4TP-4. ARF4TP-4 as selected concentration were injected i.p. for four times. The first administration is a day before IAV challenge and others are conducted within the consecutive days post IAV intranasal inoculation. Body weight of infected mice was daily monitored till 15 days p.i. and percentage of body weight was measured as an index of IAV infection. Mice were sacrificed at day 3 and 6 p.i. for tissue collection and detection according to experimental demands.

Modelling Human ARF4 and targeting Peptide Complexes

It has been reported that Arf4 and rhodopsin bind the regulatory N-terminal dimerization and cyclophillin-binding (DCB)-homology upstream of Sec7 (HUS) domain of GBF1[25]. To establish the models of human ARF4 in complex with GBF1 and ARF4 targeting peptide-ARF4TP-4, molecular docking was used. Firstly, the crystal structure of inactive human ARF4 (PDB ID: 1Z6X)[42] was downloaded from RCSB PDB Bank (http://www.rcsb.org). Secondly, the active human ARF4 was built based on a template from yeast ARF1 (PDB ID: 2KSQ). Thirdly, the AlphaFold-predicted structure of human GBF1 was downloaded from UniProt (UniProt ID: Q92538). Fourthly, the active ARF4-GBF1 complex structure was built based on a template Arf1-Brag2 complex (PDB ID: 4C0A). Fifthly, the active site of ARF4TP-4 was identified according to the previous study, in which α helix 3 of ARF4 was proposed as interacting partner of rhodopsin C terminus, the VXPX-COOH motif[43]. Finally, ARF4TP-4 were docked into the active site with AutoDockTools[44] and CUDA-accelerated AutoDock-GPU[45]. The 2D protein-ligand interaction were analyzed by LigPlot+ (version 2.2.4)[46]. The 3D visualization and plot were generated by ChimeraX[47].

Statistics and reproducibility

Statistical analyses were performed with GraphPad Prism software. In all figures, the datapoints and bar graphs represent the mean of independent biological replicates. In all graphs, the error bars represent the standard deviation and are only shown for experiments with n = 3 or greater as indicated. For microscopy experiments, data sets for quantitative analysis were acquired from an average of 40–50 fields from four to five independent

reproducible experiments for each condition. Comparisons between control and sample datapoints were made using either the Student's unpaired t test, or two-way ANOVA with Dunnett's multiple-comparison analyses, or other statistics methods as specified in the figure legends with a confidence limit for significance set at 0.05 or less.

Reference

1 Guzman, M. G. et al. Dengue: a continuing global threat. Nat. Rev. Microbiol. 8, S7-16, doi:10.1038/nrmicro2460.(2010)

2 Lessler, J. et al. Assessing the global threat from Zika virus. Science 353, aaf8160, doi:10.1126/science.aaf8160 (2016).

3 Eccleston-Turner, M., Phelan, A. & Katz, R. Preparing for the Next Pandemic - The WHO's Global Influenza Strategy. N. Engl. J. Med. 381, 2192-2194, doi:10.1056/NEJMp1905224 (2019).

4 Wu, F. et al. (2020) A new coronavirus associated with human respiratory disease in China. Nature 579, 265-269, doi:10.1038/s41586-020-2008-3.

5 Ventura, C. V., Maia, M., Bravo-Filho, V., Gois, A. L. & Belfort, R., Jr. (2016) Zika virus in Brazil and macular atrophy in a child with microcephaly. Lancet 387, 228, doi:10.1016/S0140-6736(16)00006-4.

6 Shi, M. et al. The evolutionary history of vertebrate RNA viruses. (2018) Nature 556, 197-202, doi:10.1038/s41586-018-0012-7.

7 Cui, J., Li, F. & Shi, Z. L. Origin and evolution of pathogenic coronaviruses. (2019) Nat. Rev. Microbiol. 17, 181-192, doi:10.1038/s41579-018-0118-9.

8 Xiong, R. et al. (2020) Novel and potent inhibitors targeting DHODH are broad-spectrum antivirals against RNA viruses including newly-emerged coronavirus SARS-CoV-2. Protein Cell 11, 723-739, doi:10.1007/s13238-020-00768-w.

9 Kaur, H. et al. (2021) Efficacy and safety of dihydroorotate dehydrogenase (DHODH) inhibitors "leflunomide" and "teriflunomide" in Covid-19: A narrative review. Eur. J. Pharmacol. 906, 174233, doi:10.1016/j.ejphar.2021.174233.

10 Lin, K. & Gallay, P.(2013) Curing a viral infection by targeting the host: the example of cyclophilin inhibitors. Antiviral Res. 99, 68-77, doi:10.1016/j.antiviral.2013.03.020.

11 Zumla, A., Chan, J. F., Azhar, E. I., Hui, D. S. & Yuen, K. Y. (2016) Coronaviruses - drug discovery and therapeutic options. Nat. Rev. Drug Discov. 15, 327-347, doi:10.1038/nrd.2015.37.

12 Li, G., Hilgenfeld, R., Whitley, R. & De Clercq, E. (2023) Therapeutic strategies for COVID-19: progress and lessons learned. Nat. Rev. Drug Discov. 22, 449-475, doi:10.1038/s41573-023-00672-y.

13 Shie, J. J. & Fang, J. M. (2019) Development of effective anti-influenza drugs: congeners and conjugates - a review. J. Biomed. Sci. 26, 84, doi:10.1186/s12929-019-0567-0.

14 Donaldson, J. G. & Jackson, C. L. (2011) ARF family G proteins and their regulators: roles in membrane transport, development and disease. Nat. Rev. Mol. Cell. Biol. 12, 362-375, doi:10.1038/nrm3117.

15 Cohen, L. A. & Donaldson, J. G. (2011) Analysis of Arf GTP-binding protein function in cells. Curr. Protoc. Cell. Biol. Chapter 3, Unit 14 12 11-17, doi:10.1002/0471143030.cb1412s48.

16 Verheije, M. H. et al. (2008) Mouse hepatitis coronavirus RNA replication depends on GBF1-mediated ARF1 activation. PLoS. Pathog. 4, e1000088, doi:10.1371/journal.ppat.1000088.
17 Dorobantu, C. M. et al. (2014) Recruitment of PI4KIIIbeta to coxsackievirus B3 replication organelles is independent of ACBD3, GBF1, and Arf1. J. Virol. 88, 2725-2736, doi:10.1128/JVI.03650-13.
18 Wang, P. G. et al. (2009) Efficient assembly and secretion of recombinant subviral particles of the four dengue serotypes using native prM and E proteins. PLoS One 4, e8325, doi:10.1371/journal.pone.0008325.
19 Kudelko, M. et al. (2021) Class II ADP-ribosylation Factors Are Required for Efficient Secretion of Dengue Viruses. J. Biol. Chem. 287, 767-777, doi:M111.270579 [pii] 10.1074/jbc.M111.270579.
20 Chan, J. F. et al. (2016) Zika Virus Infection in Dexamethasone-immunosuppressed Mice Demonstrating Disseminated Infection with Multi-organ Involvement Including Orchitis Effectively Treated by Recombinant Type I Interferons. EBioMedicine 14, 112-122, doi:10.1016/j.ebiom.2016.11.017.
21 Li, M. Y. et al. (2020) Lyn kinase regulates egress of flaviviruses in autophagosome-derived organelles. Nat. Commun. 11, 5189, doi:10.1038/s41467-020-19028-w (2020).
22 Li, M. Y. et al. KDEL Receptors Assist Dengue Virus Exit from the Endoplasmic Reticulum. Cell reports, doi:10.1016/j.celrep.2015.02.021.
23 Thangavel, R. R. & Bouvier, N. M. (2014) Animal models for influenza virus pathogenesis, transmission, and immunology. J. Immuno.l Methods 410, 60-79, doi:10.1016/j.jim.2014.03.023.
24 Bouvier, N. M. & Lowen, A. C. (2010) Animal Models for Influenza Virus Pathogenesis and Transmission. Viruses 2, 1530-1563, doi:10.3390/v20801530.
25 Wang, J., Fresquez, T., Kandachar, V. & Deretic, D. (2017) The Arf GEF GBF1 and Arf4 synergize with the sensory receptor cargo, rhodopsin, to regulate ciliary membrane trafficking. J. Cell Sci. 130, 3975-3987, doi:10.1242/jcs.205492.
26 Bonifacino, J. S. & Glick, B. S. (2004) The mechanisms of vesicle budding and fusion. Cell 116, 153-166, doi:10.1016/s0092-8674(03)01079-1.
27 Mellman, I. & Warren, G. (2000) The road taken: past and future foundations of membrane traffic. Cell 100, 99-112, doi:10.1016/s0092-8674(00)81687-6.
28 Roth, A. N. et al. (2021) Ins and Outs of Reovirus: Vesicular Trafficking in Viral Entry and Egress. Trends Microbiol. 29, 363-375, doi:10.1016/j.tim.2020.09.004.
29 Hassan, Z., Kumar, N. D., Reggiori, F. & Khan, G. (2021) How Viruses Hijack and Modify the Secretory Transport Pathway. Cells 10, doi:10.3390/cells10102535.
30 Coller, K. E. et al. (2012) Molecular determinants and dynamics of hepatitis C virus secretion. PLoS Pathog. 8, e1002466, doi:10.1371/journal.ppat.1002466.
31 zur Wiesch, P. A., Kouyos, R., Engelstadter, J., Regoes, R. R. & Bonhoeffer, S. (2011) Population biological principles of drug-resistance evolution in infectious diseases. The Lancet. Infect. Dis. 11, 236-247, doi:10.1016/S1473-3099(10)70264-4.
32 Barrows, N. J. et al. (2016) A Screen of FDA-Approved Drugs for Inhibitors of Zika Virus Infection. Cell Host Microbe 20, 259-270, doi:10.1016/j.chom.2016.07.004.
33 Chun, J., Shapovalova, Z., Dejgaard, S. Y., Presley, J. F. & Melancon, P. (2008) Characterization of class I and II ADP-ribosylation factors (Arfs) in live cells: GDP-bound class II Arfs associate with the ER-Golgi intermediate compartment independently of GBF1. Mol. Biol. Cell 19, 3488-3500, doi:10.1091/mbc.E08-04-0373.

34 Duijsings, D. et al. (2009) Differential membrane association properties and regulation of class I and class II Arfs. Traffic 10, 316-323, doi:10.1111/j.1600-0854.2008.00868.x.
35 BuNakai, W. et al. (2013) ARF1 and ARF4 regulate recycling endosomal morphology and retrograde transport from endosomes to the Golgi apparatus. Mol. Biol. Cell 24, 2570-2581, doi:10.1091/mbc.E13-04-0197.
36 Robinson, S. M. et al. (2014) Coxsackievirus B exits the host cell in shed microvesicles displaying autophagosomal markers. PLoS Pathog. 10, e1004045, doi:10.1371/journal.ppat.1004045.
37 Chen, Y. H. et al. (2015) Phosphatidylserine vesicles enable efficient en bloc transmission of enteroviruses. Cell 160, 619-630, doi:10.1016/j.cell.2015.01.032.
38 Mutsafi, Y. & Altan-Bonnet, N. (2018) Enterovirus Transmission by Secretory Autophagy. Viruses 10, doi:10.3390/v10030139.
39 Ghosh, S. et al. (2020) beta-Coronaviruses Use Lysosomes for Egress Instead of the Biosynthetic Secretory Pathway. Cell 183, 1520-1535 e1514, doi:10.1016/j.cell.2020.10.039.
40 Xia, B. et al. (2023) Extracellular vesicles mediate antibody-resistant transmission of SARS-CoV-2. Cell Discov. 9, 2, doi:10.1038/s41421-022-00510-2 (2023).
41 Zhao, Y. et al. Cryo-EM structures of apo and antagonist-bound human Cav3.1. Nature 576, 492-497, doi:10.1038/s41586-019-1801-3.
42 Deretic, D. et al. (2005) Rhodopsin C terminus, the site of mutations causing retinal disease, regulates trafficking by binding to ADP-ribosylation factor 4 (ARF4). Proc. Natl. Acad. Sci.USA 102, 3301-3306, doi:doi:10.1073/pnas.0500095102.
43 Morris, G. M. et al. (2009) AutoDock4 and AutoDockTools4: Automated Docking with Selective Receptor Flexibility. J. Comput. Chem. 30, 2785-2791, doi:10.1002/jcc.21256.
44 Santos-Martins, D. et al. (2021) Accelerating AutoDock4 with GPUs and Gradient-Based Local Search. J. Chem. Theory Comput. 17, 1060-1073, doi:10.1021/acs.jctc.0c01006.
45 Laskowski, R. A. & Swindells, M. B. (2011) LigPlot+: Multiple Ligand–Protein Interaction Diagrams for Drug Discovery. J. Chem. info. Model. 51, 2778-2786, doi:10.1021/ci200227u.
46 Pettersen, E. F. et al. (2021) UCSF ChimeraX: Structure visualization for researchers, educators, and developers. Protein Sci. 30, 70-82, doi:https://doi.org/10.1002/pro.3943.

Acknowledgement

We thank Prof. Lu Lu for help discussion and critical reagents. This study was supported by the National Key Research and Development Project of China (2022YFC2303700), the National Natural Science Foundation of China (82172271) to M.Y.L. and State Key Laboratory of Pathogen and Biosecurity (SKLPBS2019). P.H.C. was supported by the University Grants Committee's Collaborative Research Fund (C6036-21G), General Research Fund (16301319). Y.Q.D was supported by the Key-Area Research and Development Program of Guangdong Province (2022B1111020002). Works in the Sanyal lab is supported by the Welcome Trust (220776/Z/20/Z and 223107/Z/21/Z to SS and 225010/Z/22/Z to VS). C.F.Q. was supported by the National Science Fund for Distinguished Young Scholar (81925025) and the Innovation Fund for Medical Sciences (2019-I2M-5-049) from the Chinese Academy of Medical Sciences.

Author contributions

C.F.Q., S.S. and M.Y.L. conceived the study and wrote the manuscript. M.Y.L., K.D., X.H.C., L.Y.L.S., T.S.N., V.G.S., Q.W.T., S.V.L., H.H.W., Y.L., N.N.Z., Y.Z., T.S.C., F.Y., and Y.Q.D. conducted and analyzed the experiments. P.P.H.C., Z.R.G. performed transcriptome profiles analysis. All authors reviewed and approved the manuscript.

Competing interests

C.F.Q. and M.Y.L. have filed a patent related to the finding reported in this paper.

Main figure titles and legends

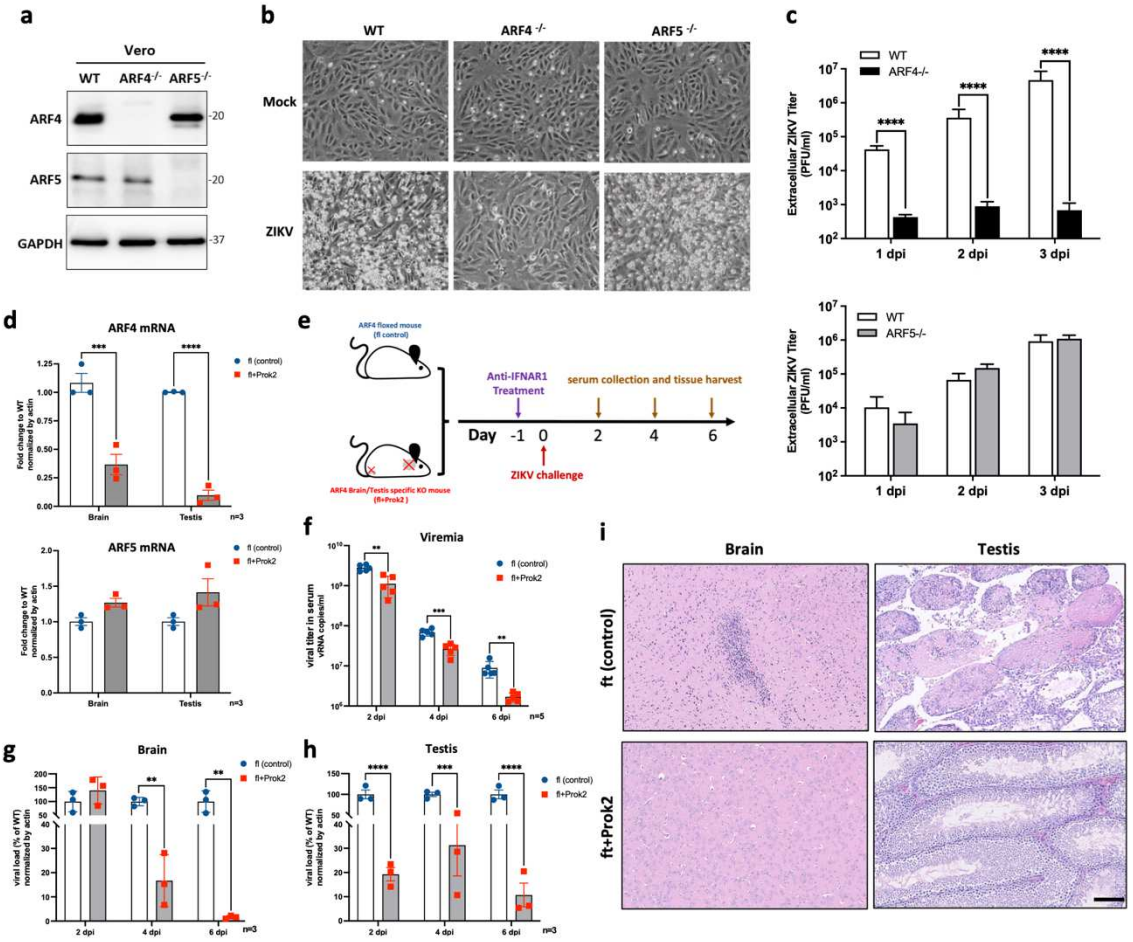

Fig. 1 ARF4 facilitates ZIKV infection, as well as leads to pathogenic outcomes a) ARF4 and ARF5 were completely deleted in Vero cells by CRISPR-Cas9 mediated knockout (ARF4$^{-/-}$ and ARF5$^{-/-}$). Cell lysates (CL) from knockout and wild type (WT) cells were collected to verify the deletion efficiency by Western blotting (WB) with the ARF4 and ARF5 specified antibodies. GAPDH was used as loading control. **b-c)** ARF4 deletion , but not ARF5 blocked ZIKV infection. ARF4$^{-/-}$, ARF5$^{-/-}$ and WT Vero cells were challenged with ZIKV at MOI of 0.1. Culture medium was collected daily until cytopathic effects were observed in WT cells which appeared at day 3 days post infection (dpi) shown in B). Viral titers were determined by plaque assay on Vero cells and expressed as PFU/ml. **d)** Transcription of endogenous ARF4 was detected by RT-qPCR using total RNA isolated from brain and testis collected from C57BL/6JGpt based control ARF4-flox (fl control) and knockout ARF4-flox/cre-Prok2 (fl+Prok) mice. **e)** Schematic diagram of ARF4 brain/testis-specific knock-out mice with ZIKV challenge and detection. **F-h)** ZIKV infection is supressed in fl+Prok mice. Serum, as well as brain and testis were collected from

ZIKV infected fl+ProK2 and fl (control) mice at indicated dpi. Total RNA was extracted as a template to calculate viral load by performing RT-qPCR . **i)** ZIKV induced pathological changes were absent in fl+ProK2 mice. ZIKV infected brains and testis were collected and fixed at 6 dpi, then stained with hematoxylin and eosin (H&E) and examined by light microscopy observation. Above data are shown as mean ± SD **P<0.01, ***P<0.001 and ****P<0.0001 vs WT or fl (control) by the two-way ANOVA with multiple comparisons. H&E images are representative of three mice. Scale bar, 100μm.

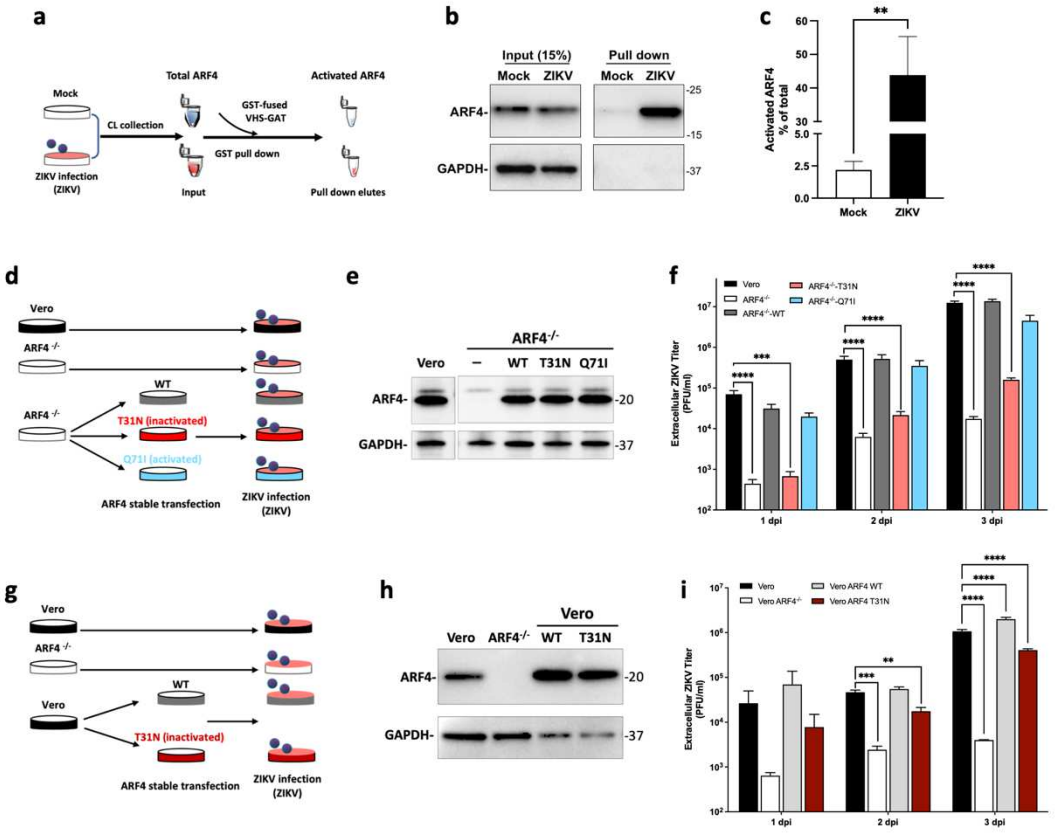

Fig. 2 Activation of ARF4 is stimulated during ZIKV infection and in turn, is essential for the production of progeny virions. a) Schematic diagram of ARF4 activation detection by VHS-GAT fused GST pull down. **B-c)** ZIKV infection stimulated ARF4 activation. Cell lysates (CL) were collected from mock or ZIKV infected (MOI=5, 30hrs) to perform GST pull down using GST fused VHS-GAT bait. CL and Final elutes, as input and pull down respectively, were subjected to WB by antibody against ARF4 and GAPDH as loading control. The activity of ARF4 was calculated as the percentage of activated ones in final elutes of total ones in CL. The data are shown as mean ± SD **P<0.05 vs mock infection by the Student's unpaired t test. **d)** Schematic

diagram of ARF4 stably transfection in Vero ARF4$^{-/-}$ cells and ZIKV infection. **e)** WT ARF4 or its constantly inactive mutant (T31N) or active mutant (Q71I) were reconstituted and stably expressed in ARF4 $^{-/-}$ cells. Expression level was detected by WB using anti-ARF4 antibody. GAPDH is used as loading control here. **f)** Production of progeny virions were rescued in Vero ARF4$^{-/-}$ cells which re-expressed either WT ARF4 or Q71I mutant, but remains blockage in T31N mutant expressing cells. ZIKV infection was performed using Vero, ARF4$^{-/-}$ and reconstituted cells (MOI=0.1). Supernatant (SN) were daily collection till 3 days p.i. to do viral titration by plaque assay. **G-i)** WT and T31N ARF4 stably overexpressed Vero cells were established and infected by ZIKV (MOI=0.1). ARF4 expression and viral titration were detected by WB and plaque assay respectively.. Results in F) and I) are means ±SD. **P<0.01,***P<0.001, ****P<0.0001 Vs Vero (same collection day) by two-way ANOVA with multiple comparisons.

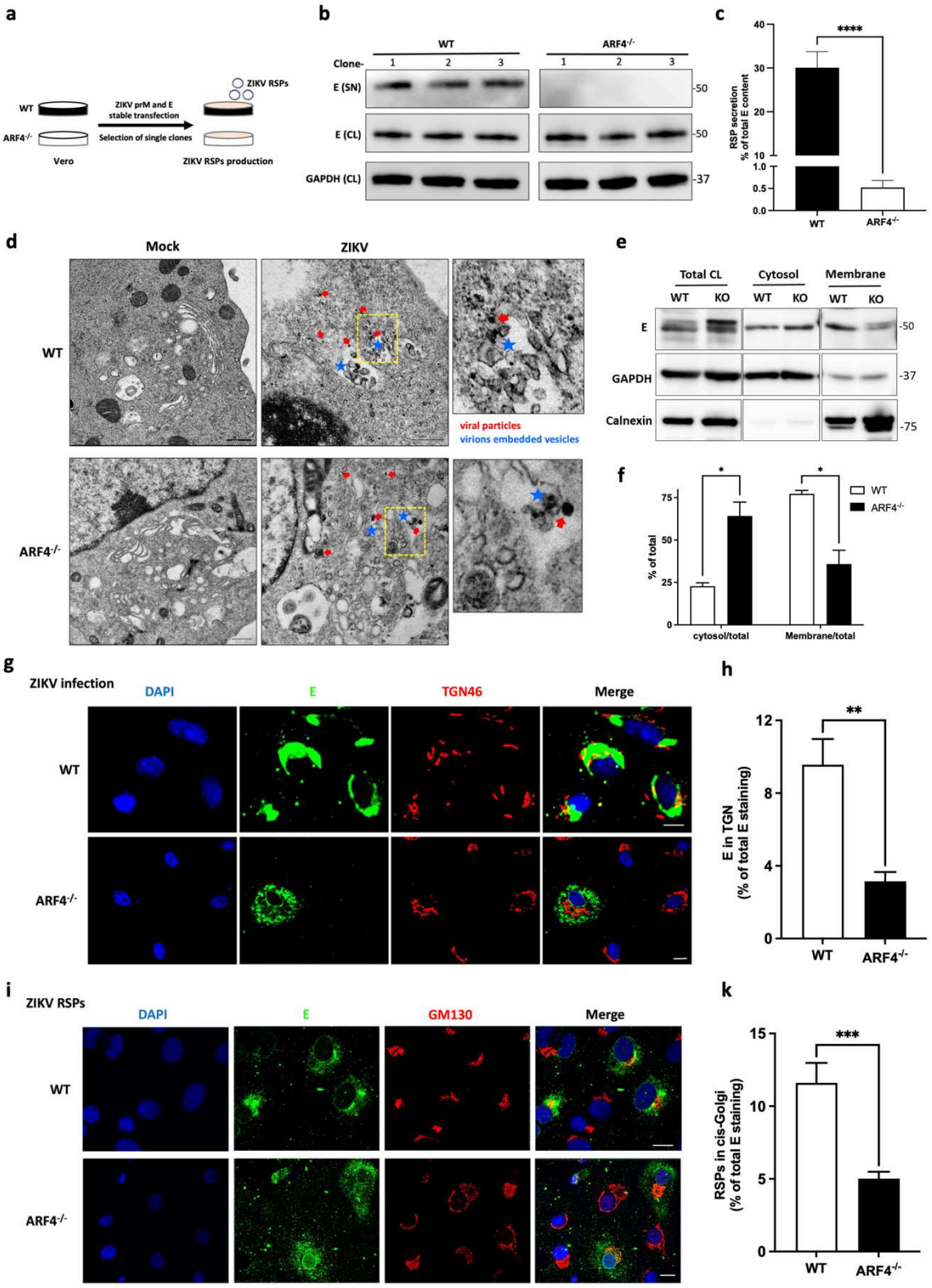

700

701 **Fig. 3 ARF4 is essential for viral egress and its deficiency interferes with viral intracellular**
702 **translocation to Golgi complex. a)** Schematic diagram of generation of ZIKV recombinant
703 subviral particles (RSPs) stably producing cells. **b-c)** ARF4 deletion extremely blocked RSPs

secretion. Single clones (-1, 2 and 3) of either Vero WT-ZIKV prME or Vero ARF4$^{-/-}$ -ZIKV prME were pick up and maintained separately. Supernatant (SN) and cell lysate (CL) were collected to perform WB. E protein was detected by using it specific antibody. GAPDH was used here as a loading control. Percentage of E(SN) in total E(SN+CL) was measured as an index of RSPs secretion. **d)** ARF4 deletion does not affect viral assembly. ZIKV infection was performed in Vero WT and ARF4$^{-/-}$cells （MOI=10 24hrs）. Cells were fixed and viral particle were visualized by transmission electron microscopy (TEM). Newly formed virions were pointed by red arrow and ER invagination-induced vesicles containing viral particles were pointed by blue star. Scale bar, 500nm **e-f)** More virions were detected in cytosol fraction isolated from ARF4$^{-/-}$ cells. Freeze-and-thaw (F&T) was performed as described in method section using prM and E expressing Vero WT and ARF4$^{-/-}$ cells. E protein was detected in isolated cytosol and membrane fraction as an index of formed RSPs and unpacked membrane viral protein respectively. GAPDH and Calnexin were detected as cytosol and membrane marker. Percentage of E measured from cytosol fraction relative to the total amount (cytosol+membrane) was used as an index of RSPs formation. Unpacked E from membrane fraction was presented as the percentage of E from membrane fraction relative to the total amount. **g-k)** ARF4 deletion arrested the ER-to-Golgi complex transport of newly formed virions. Viral E protein was co-stained with TGN46 indicated trans-Golgi network (TGN) or GM103 indicated cis-Golgi by their specific antibodies respectively in ZIKV infected Vero cells (MOI=10 36hrs)(G) or RSPs production cells (I). Scale bar=10μM. The percentage of E protein in TGN or cis-Golgi was presented as the weighted co-localization coefficients of E staining in TGN46 or GM130 stained areas by using imaging analysis software-ZEN2012 (Carl Zeiss) from over hundreds cells per conditions. TME and IFA images are representative of at least three independent experiments. Above results are means ±SD *P<0.05, **P<0.01, ***P<0.001 and ****P<0.0001 Versus untreated control or WT by the Student's unpaired t test or two-way ANOVA with multiple comparisons.

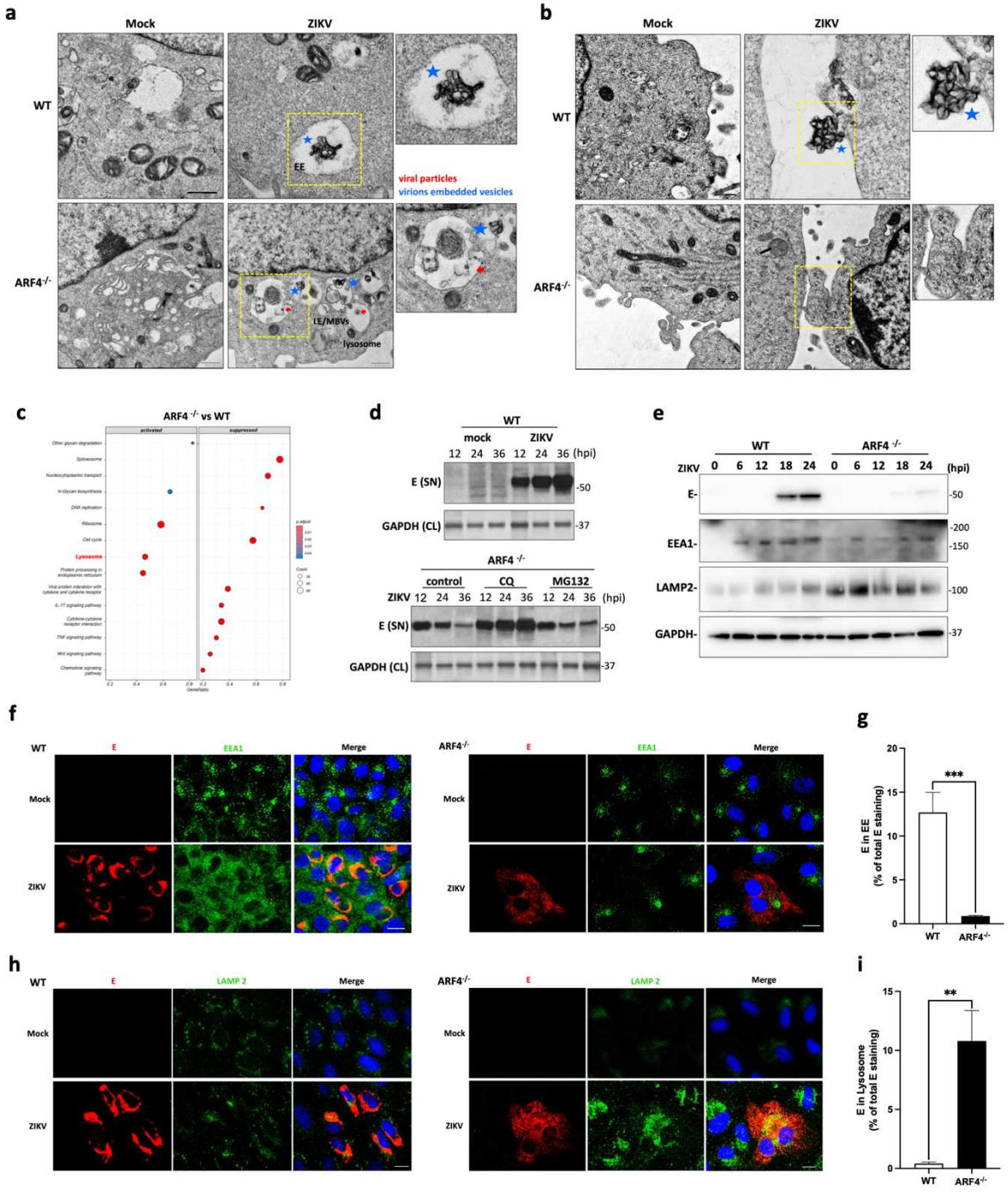

730

731 **Fig. 4 Absence of endogenous ARF4 caused the mis-sorting of newly formed viral particles**
732 **into the lysosomal degradation pathway.** TEM observation was performed with the same
733 cells as above described. **a)** Accumulated virions contained vesicles were easily visualized in
734 early endosome like compartment in ZIKV infected Vero WT cells (blue star pointed).
735 Dispersed unpacked virions were more visualized in late endosome (LE) or multivesicular
736 bodies (MVBs) like compartment in ARF4 deleted cells (red arrow pointed). **b)** Secretion of

progeny virions were observed by TEM in ZIKV infected Vero WT, but not in ARF4$^{-/-}$ cells. In WT cells, clusters virions embedded vesicles (blue star pointed) were observed on the surface of ZIKV infected cell surface. In ZIKV infected ARF4$^{-/-}$ cells, as well as mock infected WT and ARF4$^{-/-}$ cells, vain protrusions were observed on cell membrane. Scale bar, 500nm. **c)** Total RNA extracted from ZIKV infected Vero WT and ARF4$^{-/-}$ cells (MOI=0.1 48hrs) to perform RNA-seq. Bubble chart showed the GSEA analysis results, indicating that lysosome pathway has been activated in ARF4 knockout group compared to WT group. **d)** ZIKV egress was recovered in ARF4-deleted cells post chloroquine (CQ) or MG132 treatment. Either mock/ZIKV infected Vero WT cells or ARF4$^{-/-}$ cells which were ZIKV-infected after overnight treatment of CQ (20 μM) and MG132 (50 μM). Cells were radioactively labelled ([35S]cysteine/methionine) after infection. Supernatants were collected at indicated time for autoradiography. GAPDH in CL were detected as loading control. **e)** Time-cross collected CL from ZIKV infected Vero WT and ARF4$^{-/-}$ cells (MOI=1) was subjected to WB using antibodies against viral E, early endosome marker-EEA1 and lysosome marker-LAMP2. Results in D and E are representative of at least two independent experiments. **F-i)** Vero WT and ARF4$^{-/-}$ cells were mock or ZIKV infected (MOI=10 24hrs). Cells were then fixed and co-stained with antibodies against viral E, along with EEA1 (F), or LAMP2 (H) with their specific antibodies respectively. Nuclei were stained with DAPI. Scale bar =10 μM. Selected images are representative of at least three independent experiments. The percentage of E protein in early endosome (EE) or lysosome was presented as the weighted co-localization coefficients of E staining in EEA1 or LAMP2 stained areas by using imaging analysis software-ZEN2012 (Carl Zeiss) from over hundreds cells per conditions. Above results are means ±SD **P<0.01, and ***P<0.001 Versus untreated WT by the Student's unpaired t test.

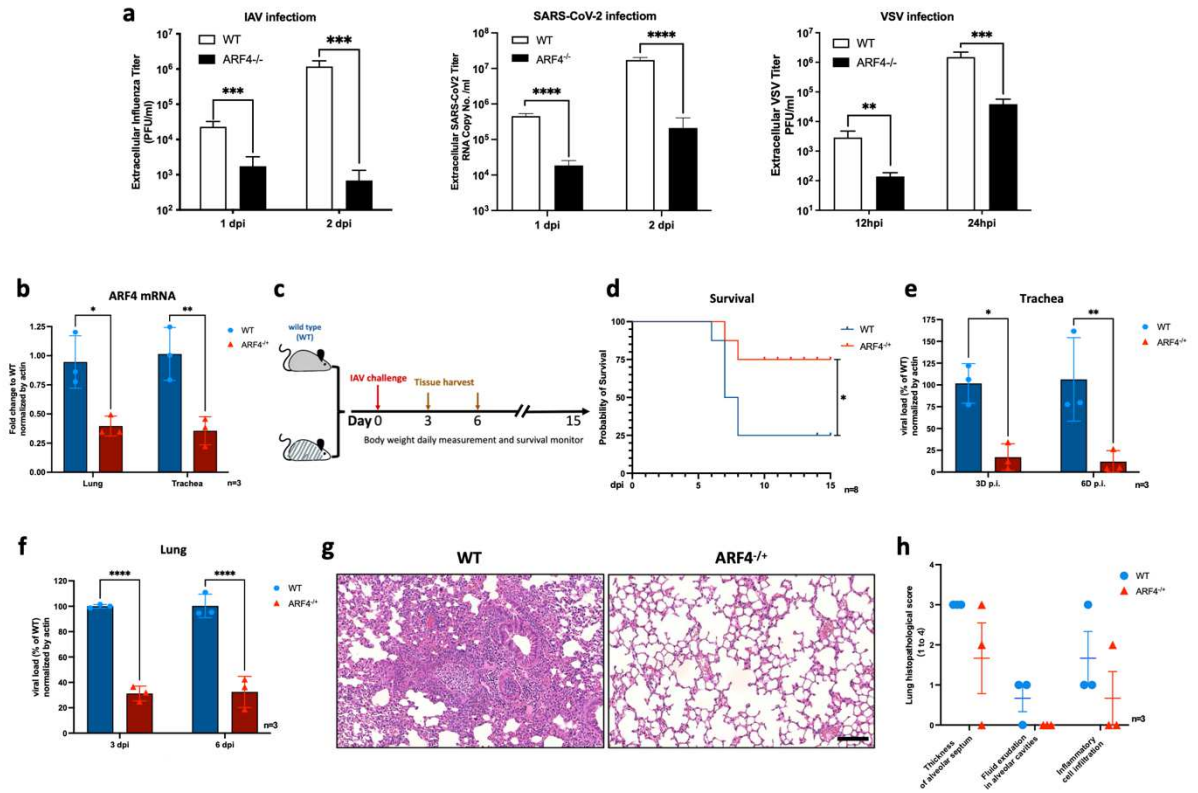

760

761 **Fig. 5 ARF4 abolishment restrained the infection and histopathological changes of other**
762 **pathogenic RNA viruses. a)** Influenza A Virus (IAV) (MOI=1), Severe acute respiratory
763 syndrome coronavirus 2 (SARS-CoV-2) (MOI=0.01) and Vesicular Stomatitis Virus (VSV)
764 (MOI=0.01) were infected in Vero WT and ARF4$^{-/-}$ cells respectively. Viral titration of IAV and
765 VSV were measured by plaque assay as PFU/ml. Viral genomic RNA of SARS-CoV-2 was
766 calculated by RT-qPCR as RNA copy No./ml. **b)** ARF4 transcription was detected by RT-qPCR
767 using total RNA isolated from lung and testis collected from WT and ARF4$^{-/+}$ mice. **c)** Schematic
768 diagram of IAV challenge and detection in WT and ARF4$^{-/+}$ mice. **d)** ARF4 deletion reduced IAV
769 induced lethal death. Survival rate was assessed to create survival curve by using Prism
770 software. *P<0.05 vs WT by Long-rank (Mantel-Cox) test. **e-f)** ZIKV infection in trachea and
771 lung was supressed in ARF4$^{-/+}$ mice. Viral load of lung and trachea at indicated days p.i. were
772 calculated by RT-qPCR using IAV specified probe and primers. **g-h)** HE staining and
773 histopathological score of IAV infected lung sections collected from WT and ARF4$^{-/+}$ mice at 6
774 dpi. Results are shown as means ± SD *P<0.05, **P<0.01, ***P<0.001 and ****P<0.0001 vs
775 WT or PBS control by two-way ANOVA with multiple comparisons. Selected HE staining images
776 were representative of three random picked mice. Scar bar,100μM.

a

Name	Sequence	CC_{50} (μM)	IC_{50} (μM)	Selectivity Index
ARF4TP-1	QVSPA	213	12.42	17.15
ARF4TP-2	SVSTSQ VSPA	256.9	64.65	3.97
ARF4TP-3	NVTPV	145.1	43.40	3.34
ARF4TP-4	QVYPL	196.2	3.25	60.37
ARF4TP-5	NVTPI	117.6	107.7	1.09

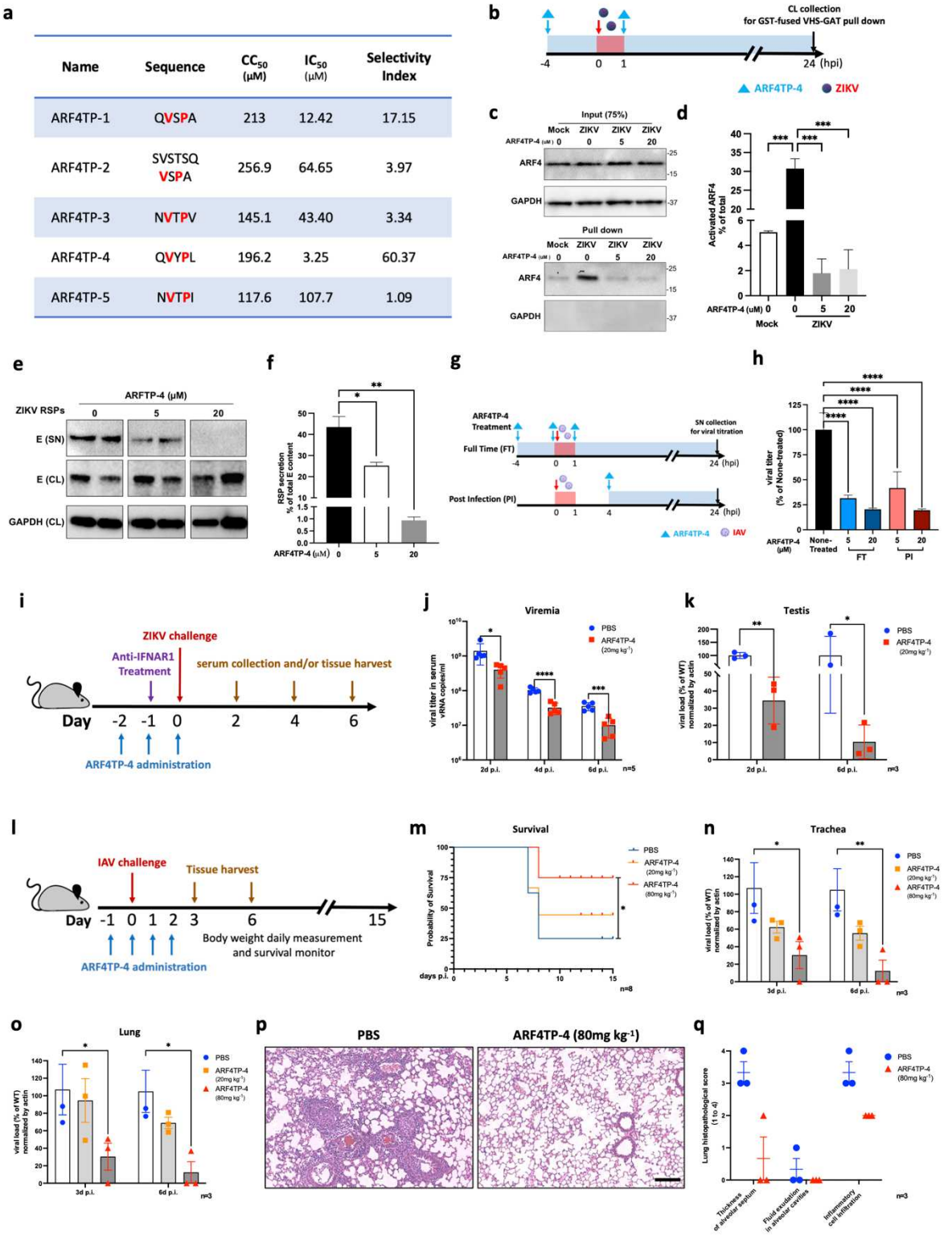

777

778 **Fig. 6 ARF4 targeting peptides, as board spectrum antivirals, efficiently arrested viral**
779 **infection both *in vitro* and *in vivo*. a)** CC_{50} and IC_{50} of ARF4 targeting peptides named ARF4TPs
780 was measured as described in method section. **b-d)** ARF4TP-4 treatment blocked ZIKV induced
781 ARF4 activation. ARF4TP-4 treatment and ZIKV challenged were performed as described in

schematic diagram. Mock infected without ARF4TP-4 treatment as a negative control. ARF4 activity was detected and measured by performing GST-VHS-GAT pull down. The data are shown as mean ± SD ***P<0.001 by two-way ANOVA. **e-f)** ARF4TP-4 arrested ZIKV RSPs secretion. Vero-ZIKV prME cells were treated with ARF4TP-4 as indicated concentration. SN and CL were collected to perform WB for RSPs secretion detection. RSPs secretion was calculated as described above. **g-h)** Vero cells were treated with ARF4TP-4 and infected by IAV (MOI=0.5) as described in schematic diagram. SN was collected for viral titration by RT-qPCR. The data are shown as mean ± SD *P<0.05 and **P<0.01 vs none-treated control by two-way ANOVA with multiple comparisons. **i)** Schematic diagram of ARFTP-4 treatment in ZIKV infected mice. **j)** ZIKV induced viremia was relieved in ARF4TP-4 treated mice. ZIKV genomic RNA in ZIKV infected mice sera were detected by RT-qPCR at indicated days p.i. **k)**. ARF4TP-4 treatment reduced ZIKV infection in testis. ZIKV infection in Viral genomic RNA copy number were measured in collected testis at indicated days after infection. **l)** Schematic diagram of ARF4TP-4 treatment in IAV infection in vivo. **m-q)** Survival curve, viral load and histopathological changes in lung were tested respectively following the similar processes described above. Results are shown as means ± SD *P<0.05, **P<0.01, ***P<0.001 and ****P<0.0001 vs PBS control by two-way ANOVA with multiple comparisons. Selected HE staining images were representative of three random picked mice. Scar bar,100 μM.

Extended Data figure titles and legends

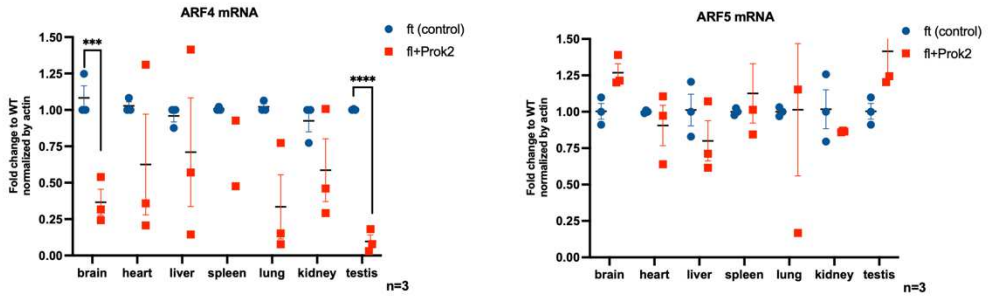

Extended Data Fig.1 Transcription of ARF4, not ARF5 was reduced in brain and testis of ARF4-flox/cre-Prok2 (fl+Prok) mice C57BL/6JGpt based control ARF4-flox (fl control) and knockout ARF4-flox/cre-Prok2 (fl+Prok) mice were generated and then collected for transcription measurement. Total RNA were isolated from indicated viral targeting tissues to be used as templates for the following RT-qPCR using ARF4 and ARF5 specific primers respectively. The data are shown as mean ± SD ***P<0.001 and ****P<0.0001 vs ft control by two-way ANOVA with multiple comparisons.

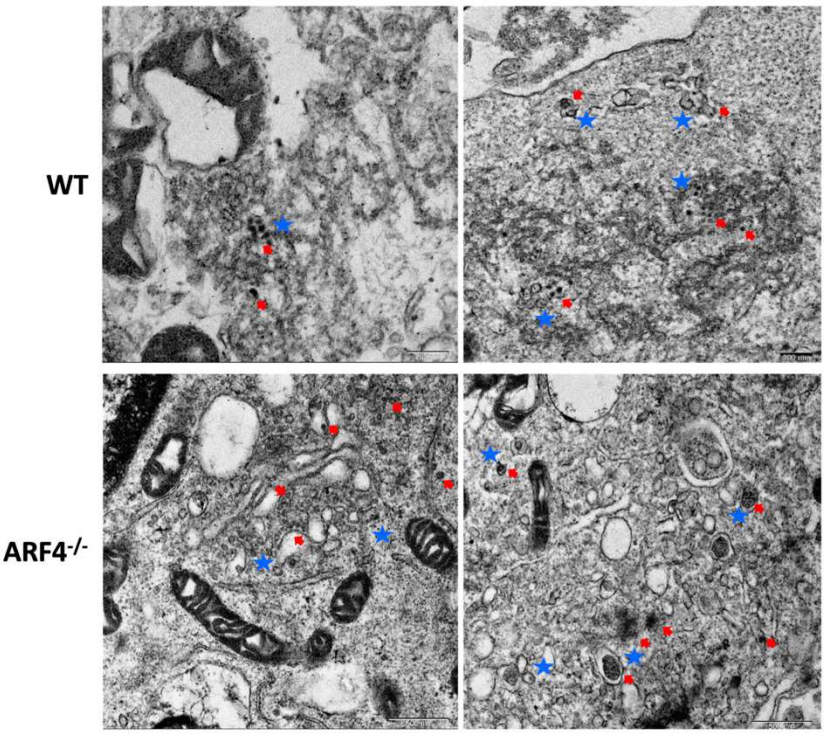

Extended Data Fig.2 Newly formed viral particles were visualized by TEM ZIKV infected Vero WT and ARF4$^{-/-}$ cells were fixed at 24hrs after infection (MOI=10) and performed TEM observation. Newly formed virions were pointed by red arrow and ER invagination-induced vesicles containing viral particles were pointed by blue star. Scale bar, 500nm.

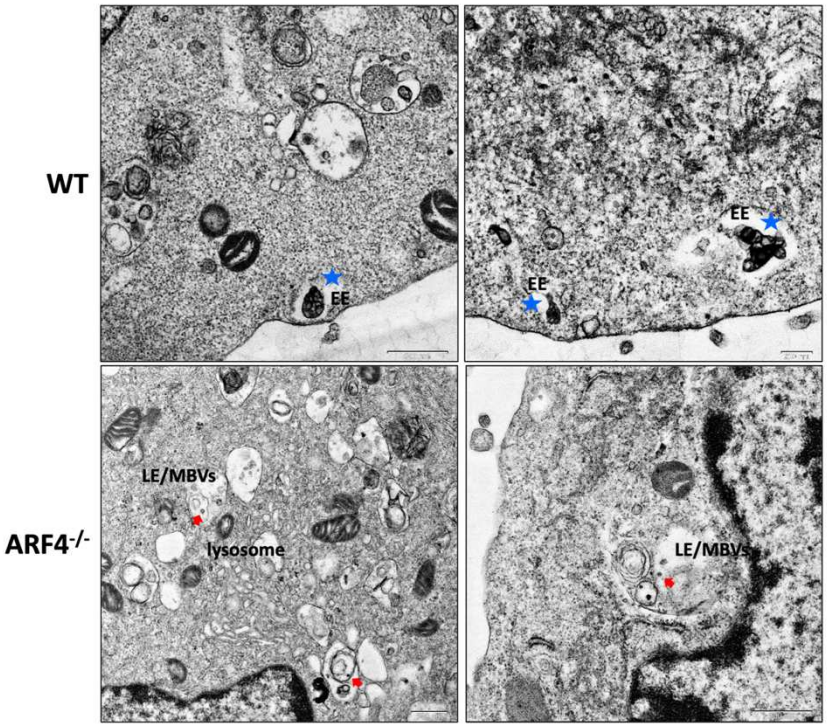

Extended Data Fig.3 ARF4 plays an important role in sorting of newly formed viral particles during their Intracellular transport ZIKV infected Vero WT and ARF4$^{-/-}$ cells were fixed at 24hrs after infection (MOI=10) and performed TEM observation. Accumulated virions were formed as a cluster which was observed in early endosome like compartments in Vero WT cells (upper panel pointed by blue star). Individual or a cluster of virions were visualized in late endosome compartment surrounding with lysosome in ARF4$^{-/-}$ cells (lower right panel pointed by red arrow).

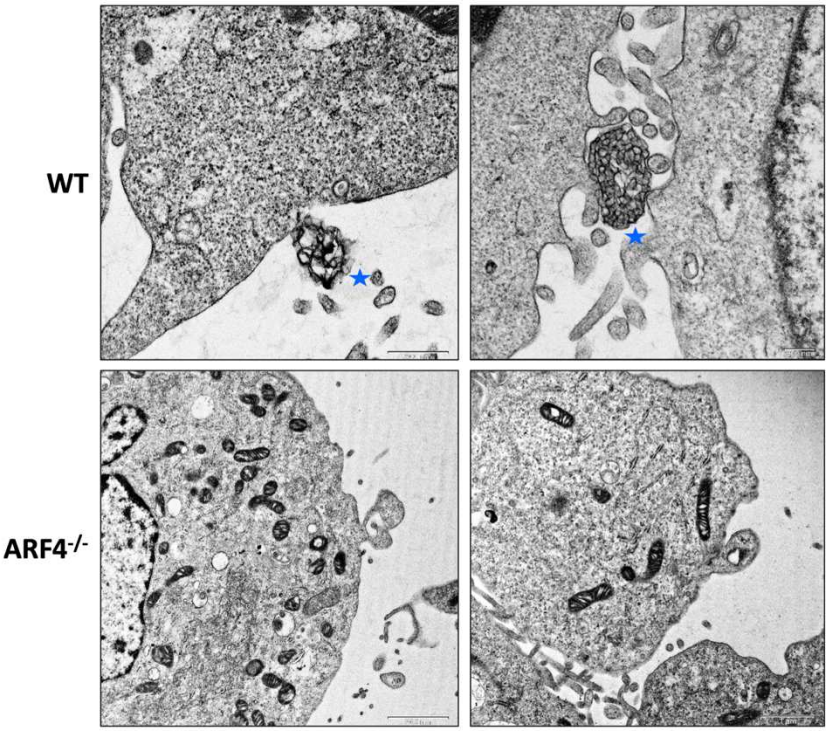

Extended Data Fig.4 Secretion of ZIKV progeny virions were observed by TEM in Vero WT, but not ARF4$^{-/-}$ cells ZIKV infected Vero WT and ARF4$^{-/-}$ cells were fixed at 24hrs after infection (MOI=10) and performed TEM observation. A cluster of membrane packed virions was observed to be budded on the cell membrane only in infected WT cells (pointed by blue star).

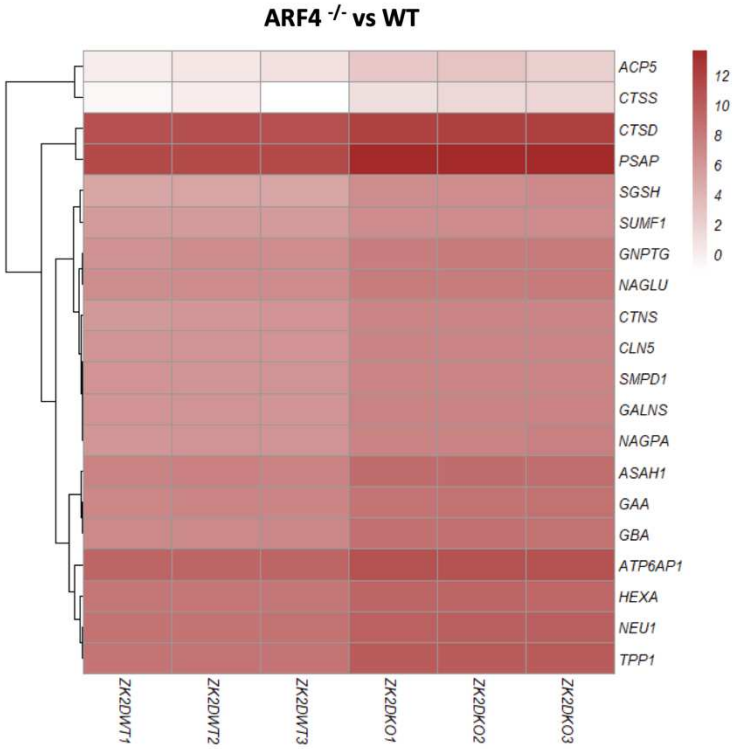

Extended Data Fig.5 Heatmap analyses indicated that top 20 genes enriched in the lysosome pathway upregulated in ARF4 knockout group compared to WT group Heatmaps of gene expression levels shows as log2(gene expression).

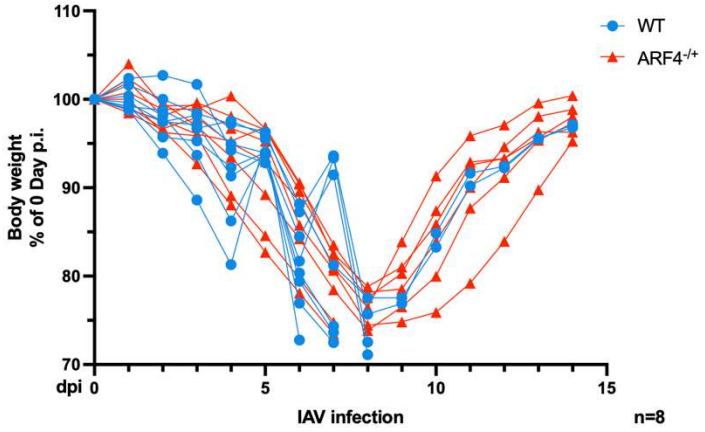

Extended Data Fig.6 Body weight lost induced by IAV were easier to be recovered in ARF4-/+ mice, related to Figure 5. Body weight was daily measured after IAV challenge in both wide-type (WT) and in ARF4-/+ mice for 14 days or till the body weight reduction was up to 25%.

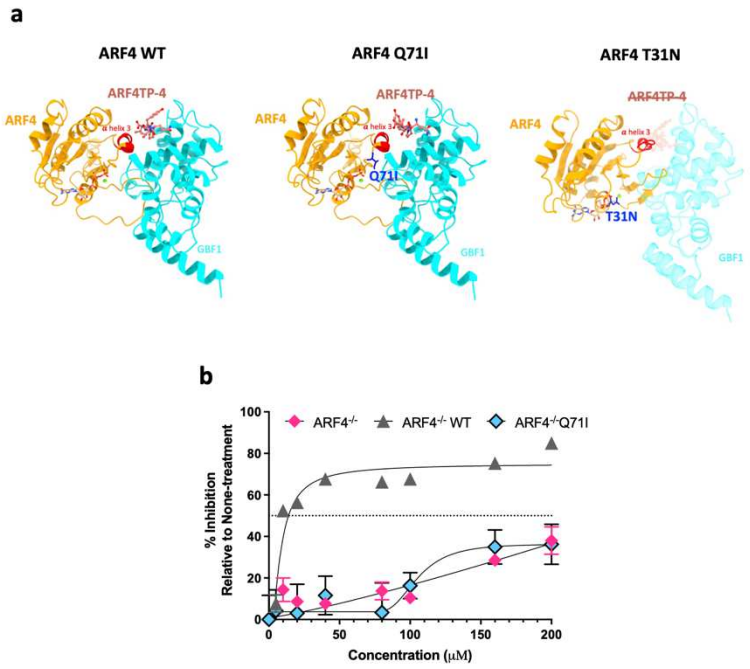

Extended Data Fig.7 Activated ARF4 mutant-Q71I was not sensitive to ARF4TP-4 treatment. **a)** The 3D visualization of putative interaction of ARF4TP-4 with human ARF4-WT, Q71I and T31N. The ARF4 WT and Q71I in active conformation or T31N in inactive conformation was rendered by cartoon and coloured in orange, in which the α helix 3 was highlighted in red. The mutated residue-Q71I or T31N was coloured in blue. The GBF1 was rendered by cartoon and

coloured in cyan. The peptide QVYPL was rendered by ball-stick and coloured in salmon. ARF4-T31N is fail to bind to ARF4TP-4, therefore the colour of GBF1 and ARF4TP-4 are turned into transparent. **b)** ARF4TP-4 treatment functions in ARF4 WT re-expressing cells but not in ARF4-deleted or Q71I re-expressing cells. Inhibition capability of ARF4TP-4 was detected following the same process to IC50 assay, but using ZIKV infected Vero ARF4-/- and re-expressed ARF4 WT or Q71I cells respectively.

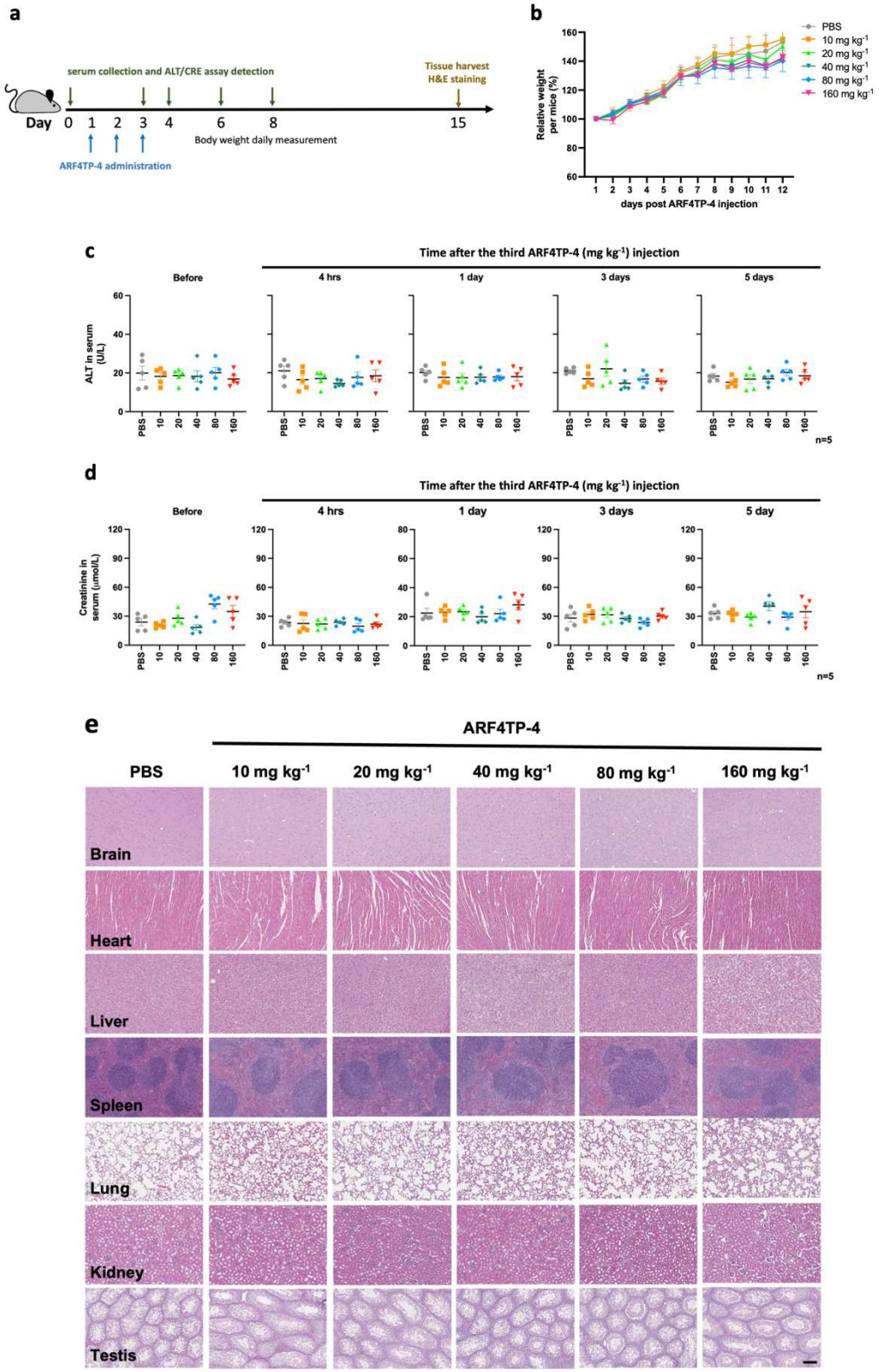

Extended Data Fig.8 ARF4TP-4 is safe for mice a) Schematic diagram of safety assay in vivo. C57BL/6 mice were assigned randomly to six groups and were injected by i.p. route with PBS (n=3), or ARF4TP-4 dissolved by PBS at escalating dose (10, 20, 40, 80 and 160 mg kg^{-1}, n=5)

daily for three consecutive days. Body weight was measured daily after third ARF4TP-4 injection. Sera were collected at indicated days for ALT and creatinine (CRE) detection. Two mice of each groups were sacrificed for tissue collection and following H&E staining**. b)** Body weight of ARF4TP-4 treated mice were not changed in comparison of PBS injection control mice. Date are means ±SD. **c)** The ALT in the sera collected at indicated day from PBS or ARF4TP-4 injection mice were measured by using the ALT assay kit (NJJCBIO). **d)** The creatinine in collected sera was measured by using the creatinine kit (NJJCBIO). All error bars reflect ±SD. **e)** ARF4TP-4 injection did not induce significant histopathological changes. Indicated tissues were collected and fixed by 4%PFA to do HE staining at 12 days post the 3rd time ARF4TP-4 injection.

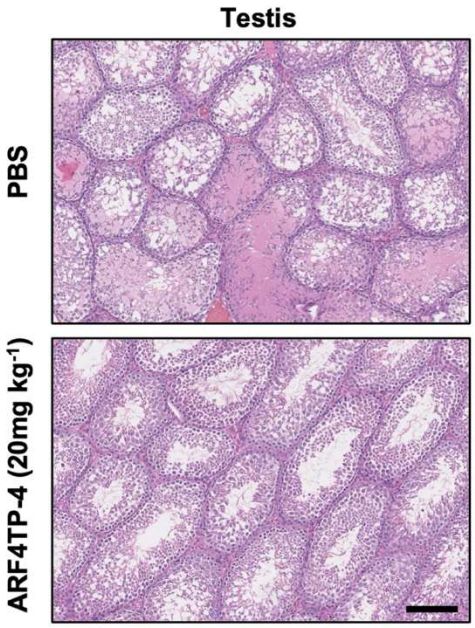

Extended Data Fig.9 ZIKV induced histopathological changes in testis were vanished after ARF4TP treatment H&E images are representative of three mice. Scale bar, 100μm.

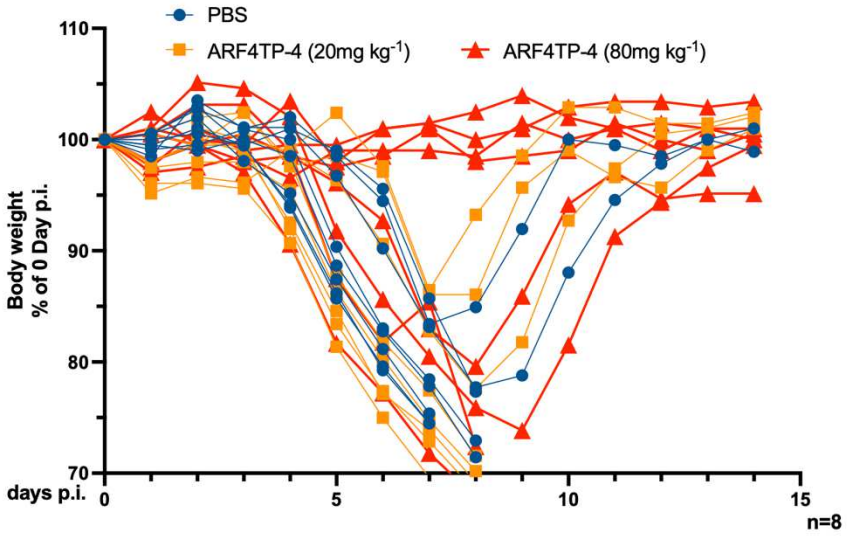

865

866 **Extended Data Fig.10 ARF4TP-4 treatment obviously prevented the body weight lost after**
867 **IAV challenge** ARF4TP-4 treatment and IAV challenge were performed as described in Fig 6f.
868 Body weight daily monitor was performed in both wide-type (WT) and in ARF4TP-4 treated
869 mice for 14 days post IAV inoculation or till the body weight reduction was up to 25%.